Published online 24 June 2021

Nucleic Acids Research, 2021, Vol. 49, No. 13 ***7457–7475***
https://doi.org/10.1093/nar/gkab526

Impact of the interplay between stemness features, p53 and pol iota on replication pathway choices

Michaela Ihle[1], Stephanie Biber[1], Insa S. Schroeder[2], Christine Blattner[3], Miriam Deniz[1], Giovanna Damia[4], Vanesa Gottifredi[5,*] and Lisa Wiesmüller[1,*]

[1]Department of Obstetrics and Gynecology, Ulm University, Ulm 89075, Germany, [2]Department of Biophysics, GSI Helmholtz Center for Heavy Ion Research, Darmstadt 64291, Germany, [3]Institute for Biological and Chemical Systems – Biological Information Processing, Karlsruhe Institute of Technology, Karlsruhe 76021, Germany, [4]Department of Oncology, Istituto di Ricerche Farmacologiche Mario Negri-IRCCS Milan, Milan 20156, Italy and [5]Cell cycle and Genomic Stability Laboratory, Fundación Instituto Leloir, Buenos Aires C1405BWE, Argentina

Received January 18, 2021; Revised June 02, 2021; Editorial Decision June 03, 2021; Accepted June 09, 2021

ABSTRACT

Using human embryonic, adult and cancer stem cells/stem cell-like cells (SCs), we demonstrate that DNA replication speed differs in SCs and their differentiated counterparts. While SCs decelerate DNA replication, differentiated cells synthesize DNA faster and accumulate DNA damage. Notably, both replication phenotypes depend on p53 and polymerase iota (POLι). By exploring protein interactions and newly synthesized DNA, we show that SCs promote complex formation of p53 and POLι at replication sites. Intriguingly, in SCs the translocase ZRANB3 is recruited to POLι and required for slow-down of DNA replication. The known role of ZRANB3 in fork reversal suggests that the p53–POLι complex mediates slow but safe bypass of replication barriers in SCs. In differentiated cells, POLι localizes more transiently to sites of DNA synthesis and no longer interacts with p53 facilitating fast POLι-dependent DNA replication. In this alternative scenario, POLι associates with the p53 target p21, which antagonizes PCNA polyubiquitination and, thereby potentially disfavors the recruitment of translocases. Altogether, we provide evidence for diametrically opposed DNA replication phenotypes in SCs and their differentiated counterparts putting DNA replication-based strategies in the spotlight for the creation of therapeutic opportunities targeting SCs.

INTRODUCTION

Increasing evidence suggests an interplay between the DNA damage response (DDR) and the epithelial–mesenchymal transition (EMT) (1,2) a pathway activated during the acquisition of stem cell (SC) properties (3). Stem cells maintain self-renewal capacity and genomic stability by means of highly efficient DDR cascades, which lose precision when cells differentiate (4,5). While the association between DNA repair mechanisms and stemness has been intensively investigated (4), the crosstalk between SC features and other DDR mechanisms such as DNA damage tolerance (DDT) is less understood. Information was gathered mostly in the hematopoietic system using mouse models (6), and is insufficient, especially given that mice and human models differ significantly at the level of DDR activation in SCs (7,8).

Because of its role in transcriptional transactivation (TA) (9), the tumor suppressor protein p53 is a critical regulator of cancer cell plasticity (10,11), promoting differentiation of SCs (11,12), impacting on lineage choice (13) and repressing EMT (14). However, p53 also maintains the self-renewal capacity of human hematopoietic SCs (HSCs) (15), suggesting opposed functions of p53 in stem and differentiated cells. Interestingly, a TA-independent DDT role of p53 possibly involving the formation of a p53–POLι complex has been reported in cycling HSCs and progenitors (HSPCs) (16,17). It has been proposed that the coordination of POLι-polymerase and p53's exonuclease activities mediates idling events, i.e. iterative insertion and degradation of nucleotides, a function achieved by some other DNA polymerases (18). Idling generates a dynamic stalling, which correlates with augmented poly-ubiquitination of proliferating cell nuclear antigen (PCNA) by the ubiquitin ligase Rad5-related helicase-like transcription factor (HLTF) and involves the SWI/SNF catalytic subunit (SNF2) translocase zinc finger ran-binding domain containing 3 (ZRANB3). Given the established role of ZRANB3 in fork reversal (19) it is most likely that the p53–POLι idling pathway involves fork reversal (FR) events.

Herein we explore the relevance of p53 for DDT in stem and differentiated cells, focusing on the role of the p53–

*To whom correspondence should be addressed. Tel: +49 731 500 58800; Fax: +49 731 500 58804; Email: lisa.wiesmueller@uni-ulm.de
Correspondence may also be addressed to Vanesa Gottifredi. Tel: +5411 52387500; Fax: +5411 52387501; Email: vgottifredi@leloir.org.ar

POLι pathway. When analyzing replication phenotypes in human embryonic, adult and cancer SCs and differentiated counterparts, we revealed an unexpected association between the differentiation stage and the DDT pathway choice. Remarkably, p53 and POLι are key for both choices. While SCs engaged a p53–POLι mediated DDT, differentiated cells are biased towards a faster bypass mechanism that does not depend on the p53–POLι complex, but depends on each protein individually.

MATERIALS AND METHODS

Please refer to Supplementary Material and Methods for further details.

Cell cultures

All cells were cultured at 37°C, 5% CO_2 and ambient O_2. Ovarian cancer cell differentiation was induced by removal of growth factors and addition of 10% FBS (Merck, Darmstadt, Germany) for seven days as described in Ricci *et al.* (20). HSPCs and PBLs were isolated from cord blood samples with consent of the parents and the approval by the local advisory boards (approval #155/13 from the Ethical Board of Ulm University). Human embryonic stem cells (hESCs) were cultured as in Luft *et al.* (21) and experiments were performed in the laboratories of the GSI Helmholtz Center for Heavy Ion Research, Darmstadt, Germany in the Group of Stem Cell Differentiation and Cytogenetics, Department of Biophysics (authorization numbers 3.0402/0069 and 3.04.02/006-E01) supervised by Insa Schroeder. Further details of isolation of hematopoietic cells as well as cell culturing of hESCs are described in the Supplementary Material and Methods.

Transfection

The plasmids as well as siRNAs, which were used for cell transfection are described in detail in the Supplementary Material and Methods.

hESCs were transfected using siRNAs and HiPerFect (Qiagen, Hilden, Germany). After 24 h medium was changed and after in total 48 h the experiments were conducted.

Silencing of p53 and POLι in HSPCs and PBLs was achieved by nucleofection with the Amaxa Human B cell nucleofector solution (Lonza, Walkersville, Maryland, USA) and the Amaxa Device II (Lonza). 1×10^6 cells were mixed with 10μg plasmid and 100μl Amaxa nucleofector solution. After applying program U-008 for HSPCs or U-015 for PBLs, HSPCs were immediately transferred to their standard medium, whereas PBLs were cultured in RPMI medium (Gibco by Thermo Fisher Scientific, Waltham, Massachusetts, USA) containing 1% (v/v) Penicillin/Streptomycin (Gibco by Thermo Fisher Scientific) and 20% (v/v) FBS (Biochrom by Merck, Darmstadt, Germany). 4h post-transfection 2% Phytohemagglutinin (Gibco by Thermo Fisher Scientific) was added. Experiments were carried out 24 h post-transfection.

Ovarian cancer cell lines were transfected using the Amaxa Device II and the Amaxa Cell line nucleofector Solution V (Lonza). In 100 μl nucleofector solution a total amount of 10 μg plasmid were mixed with 2×10^6 cells and transfected using program W-001. For double-kd, also 10 μg (5 + 5) plasmid were used. Cells were seeded in their standard medium und used for experiments 24 h post-transfection.

Determination of cell viability

The colorimetric 3-(4,5-dimethylthiazol-2-yl)-2,5-diphenyltetrazolium bromide (MTT) assay was used following manufacturers instruction (Sigma-Aldrich by Merck, Darmstadt, Germany). Consumption of nicotinamide adenine dinucleotide (NAD+), mainly generated during glycolysis was measured by the colorimetric 3-(4,5-dimethylthiazol-2-yl)-2,5-diphenyltetrazolium bromide (MTT) assay. MTT was performed 24 h post-transfection for measurement of the metabolic activity as indicator for cell viability. Cells were incubated with 0.5 mg/ml MTT (Sigma-Aldrich by Merck, Darmstadt, Germany) for 3 h and then fixed for 15 min with 0.04 M HCl diluted in 2-propanol solution before light absorbance was measured at 570 nm with an ELISA reader. Each data set of the cell viability measurement was normalized to the mean value of the corresponding control samples.

Cell cycle distribution

Propidium iodide staining was performed as previously described by us (17). To determine the fraction of cells in the different cell cycle phases, nd and diff cells were harvested and collected by centrifugation (for diff cells after trypsinization of adherently growing cells and cells floating in the supernatant). After washing with PBS and resuspension in 0.5 ml of PBS, cells were fixed by adding ice-cold 4.5 ml fixing solution (acetone and 80% (v/v) ethanol (1:1)) dropwise. Then cells were washed twice with cold PBS and resuspended in 200 μl propidium iodide staining solution (50 μg/ml PI in PBS) supplemented with 50 μg/ml RNase A (both Sigma-Aldrich by Merck, Darmstadt, Germany). After 30 min incubation in the dark, the samples were further diluted by adding 100 μl PBS with 0.2% EDTA and measured in a FACSCalibur flow cytometer (BD Biosciences, Franklin Lakes, New Jersey, USA). Percentages of G1-, S- and G2-phase cells were calculated in the live cell fraction.

Determination of S-Phase length: CldU/IdU double labeling

The difference of S-Phase length between nd and diff cells was determined by double labelling of the cells with CldU and IdU according to the protocol of Charrasse *et al.* (2017) with EdU/BrdU double labelling (22). In brief, diff cells were grown in chamber slides (Falcon® Culture Slides 4-well, OMNILAB, Bremen, Germany) whereas nd cells were cultured in 6-well and later on spun onto poly-L-lysine coated slides via cytospinning. Cells were pulsed with 10 μM CldU for 30min. Followed by incubation in medium supplemented with 5μM thymidine for either 2, 4, 6, 8 or 10 h. Afterwards, cells were pulsed again in 10 μM IdU for 30 min. Then the cells were incubated for 1min in pre-extraction buffer (300 mM Sucrose, 50 mM NaCl, 20 mM

HEPES (pH 7.4), 3 mM $MgCl_2$, 1 mM EDTA, 0.5% (v/v) Triton X-100 in water) for diff cells directly after incubation or for nd cells after cytospinning. Cells were fixed with 3.7% formaldehyde, permeabilized for 12 min with 0.5% Triton X-100 in PBS and denatured for 20 min in 4 N HCl. Finally, cells were blocked and stained as described in the paragraph 'DNA Fiber Spreading Assay'. Cells were visualized with a BZ-9000 microscope (Keyence, Cologne, Germany) and a 40× objective. Counting of the stained cells was carried out with the Fiji (Fiji is just ImageJ) software (ImageJ Wiki, Laboratory for Optical and Computational Instrumentation, University of Wisconsin-Madison, Wisconsin, USA).

Coimmunoprecipitations

Co-IPs were performed 24 h post-seeding following previously described methods (17,23). Chromatin extracts were obtained by incubation for 12 min at 4°C with Cytoskeletal buffer (250 mM Sucrose, 25 mM KCl, 1 mM HEPES (pH 7.5), 1 mM EGTA, 1 mM $MgCl_2$ in water) with freshly added inhibitors: 1 mM phenylmethylsulfonylflouride (PMSF), 1 mM Na_3VO_4, protease inhibitor cocktail (Roche, Basel, Switzerland) and 0.1 mM dithiothreitol (DTT). Crosslinking was carried out by adding 1% (v/v) methanol-free formaldehyde in PBS and incubating for 10 min at RT. Afterwards, cells were put on ice and 10 mM cold Glycine was added for 5 min to stop crosslinking. Cells were then lysed with RIPA buffer (10 mM Tris–HCl (pH 7.5), 25 mM sodium-fluoride, 20 mM sodium-chloride, 1% (v/v) sodium-deoxycholate, 1% (v/v) Nonidet P40, 0.1% SDS in water) with freshly added protease inhibitors (mentioned above) and 0.1 mM DTT. After 15 min incubation cells were harvested and sonified in a sonification water bath Sonorex (Bandelin electronic GmbH & Co. KG, Berlin, Germany) at high power three-times each 7.5 min: 30 s on, 30 s off. Supernatant was harvested by centrifugation and used for immunoprecipitation of p53 with antibodies Pab421 (mouse, OP03, Calbiochem, Darmstadt, Germany) and Pab1801 (mouse, OP09, Calbiochem) as well as of PCNA with anti-PCNA (mouse, ab29, Abcam, Cambridge, UK). Isotype control was performed by using normal IgG (mouse, sc-2027, Santa Cruz Biotechnology, Dallas, TX, USA). Protein extracts and Protein G Sepharose beads (PGS, GE Healthcare, Munich, Germany), as well as antibodies and PGS beads were incubated overnight at 4°C. The next day protein extracts were transferred to antibody-bead mixes and rotated for another 4 h at 4°C. Afterwards beads and bound proteins were dissolved and denatured using SDS-PAGE sample buffer.

Western blot analysis

For the analysis of protein levels, cells were lysed 24–48 h post-seeding or transfection. Protein extracts were then separated electrophoretically and transferred to activated PVDF membranes. Proteins were immunodetected via chemi-luminescence (24). Briefly, for cell lysis 50 mM Tris–base (pH 7.4), 150 mM NaCl, 2 mM EGTA, 2 mM EDTA, 25 mM sodium fluoride, 25 mM β-glycerol phosphate, 0.1 mM sodium vanadate, 0.2% triton X-100 and 0.3% Nonidet P40 were used. Protein levels were adjusted and after SDS-polyacrylamide-gel electrophoresis blotted onto PVDF membranes (Amersham by GE Healthcare, Munich, Germany). The antibodies, which were used for protein detection are described in detail in the Supplementary Material and Methods section. Chemiluminescence detection of protein levels as well as quantification of band intensities were done in the linear range using ImageLab software on a ChemiDocMP system (Bio-Rad Laboratories, Munich, Germany). Values of target genes were corrected for the loading control.

Quantitative reverse transcription PCR (qRT-PCR)

For detection of special candidate genes, stemness and EMT markers quantitative PCR after reverse transcription of mRNA was used as previously described (17). Total mRNA was isolated 24 h after seeding by using the RNeasy Mini Kit (Qiagen, Hilden, Germany). Reverse transcription was performed with the help of the QuantiTect Reverse Transcription Kit (Qiagen, Hilden, Germany). For qRT-PCR TaqMan® probes were used and the SensiFASTTM Probe Lo-ROX Kit (Bioline, Memphis, Tennessee, USA). qPCR was conducted with the Viia7 RUO thermocycler (Applied Biosystems). mRNAs of the target genes were detected with TaqMan® assays (all Thermo Fisher Scientific, Waltham, MA, USA) as described in detail in the Supplementary Material and Methods section. Values of target genes were normalized to mean values of both housekeeping genes and calculated with the comparative cycle threshold method (2-ΔCt). Finally, each data set was normalized to the value of nd cells.

DNA fiber spreading assay

DNA fiber spreading assay was performed according to Speroni *et al*. (25). Cells were labelled 24–48 h post-seeding/transfection with 20 μM 5-chloro-2-deoxyuridine (CldU, Sigma-Aldrich by Merck, Darmstadt, Germany) for the indicated times, then washed with pre-warmed PBS, followed by a second labelling with 200 μM 5-iodo-2-deoxyuridine (IdU, Sigma-Aldrich). Cells were then washed, harvested and resuspended. 2500 cells per slide were lysed with 6 μl lysis buffer (0.5% SDS, 100 mM Tris–HCl (pH 7.4), 50 mM EDTA) for 6 min at RT. Slides were then tilted ∼20° to allow the spreading of DNA via gravity. After further 6min drying, DNA was fixed on the slides by incubation for 5min with methanol-acetic acid solution (3:1). When slides were dried for another 7 min they could be stored in 70% (v/v) ethanol at 4°C overnight or directly be subjected to denaturation/deproteination in 2.5 M HCl for 1h, followed by immunofluorescence staining. Blocking with 5% (w/v) bovine serum albumin in PBS for 45 min at 37°C was followed by incubation with a primary antibody mix of anti-BrdU detecting IdU (mouse, #347580, BD, Franklin Lakes, NJ, USA) and anti-BrdU detecting CldU (rat, ab6326, Abcam, Cambridge, UK) for 1 h at RT. Finally, slides were incubated with a mix of secondary antibodies, AlexaFluor555 (anti-mouse) and AlexaFluor488 (anti-rat, both secondary antibodies were from Invitrogen by Thermo Fisher Scientific, Waltham, MA, USA) for 45 min at RT. DNA fibers were visualized with a BZ-9000

microscope (Keyence, Cologne, Germany) and a 40× objective. Measurement of the DNA fiber track length was carried out with the Fiji (Fiji is just ImageJ) software (ImageJ Wiki, Laboratory for Optical and Computational Instrumentation, University of Wisconsin-Madison, WI, USA).

Immunofluorescence staining

Cells were either grown in chamber slides (Falcon® Culture Slides 4-well, OMNILAB, Bremen, Germany) or in case of suspension culture cells were spun onto poly-L-lysine coated slides via cytospinning. Following fixation and antibody staining was performed according to Hampp *et al.* (17). In brief, after a possible 1min treatment with pre-extraction buffer (ingredients see paragraph 'Determination of S-Phase length') cells were fixed in 3.7% (v/v) formaldehyde in PBS and permeabilized with 0.5% (v/v) Triton X-100 (Sigma-Aldrich by Merck, Darmstadt, Germany). After blocking with 5% (v/v) goat-serum in PBS for 1 h at RT, cells were immunostained for 1 h at 37°C. The following primary antibodies were mixed as indicated in the figures and used: anti-53BP1 (rabbit, NB100-304, Novus Biologicals, Cambridge, UK), anti-phosphohistone H2A.X (Ser139, mouse, #05-636, Merck Millipore, Darmstadt, Germany) and anti-POLι (rabbit, PA5-29442, Thermo Fisher Scientific). Afterwards, slides were incubated for 45 min at 37°C with a mix of secondary antibodies AlexaFluor555 (anti-rabbit) and AlexaFluor488 (anti-mouse, both secondary antibodies were from Invitrogen by Thermo Fisher Scientific, Waltham, MA, USA). Slides were mounted with Vectashield containing DAPI (Vector Laboratories, Burlingame, California, USA) and a coverslip. Immunofluorescence of nuclear signals was measured with a BZ-9000 microscope (Keyence, Cologne, Germany) and a 100× oil immersion objective. Automated quantification of foci was done with the BZ-II Analyzer software (Keyence). Within one data set intensity threshold and minimal foci size were maintained.

In situ proximity ligation assay

PLA was performed according to the manufacturer's instructions (DUO92002, Sigma-Aldrich by Merck, Darmstadt, Germany). Cells were grown and spun on slides as for immunofluorescence staining. Then cells were incubated for 1 min with pre-extraction buffer (for ingredients see paragraph 'Determination of S-Phase length') before they were fixed in 3.7% (v/v) formaldehyde in PBS. For PLA we used Duolink In Situ PLA Orange Kit Mouse/Rabbit (Sigma-Aldrich by Merck, Darmstadt, Germany). Slides were blocked for 1 h at RT with the blocking solution of the kit. Afterwards, cells were double-stained with a mix of primary antibodies, which are described in detail in the Supplementary Material and Methods. PLA staining was then performed using the PLA probes of the Duolink kit: PLA probe anti-rabbit PLUS (anti-rabbit IgG (H+L); DUO92002, Sigma-Aldrich by Merck, Darmstadt, Germany) and PLA probe anti-mouse MINUS (anti-mouse IgG (H+L), DUO92004, Sigma-Aldrich by Merck, Darmstadt Germany) for 1 h at 37°C. Slides were then incubated for ligation with the ligase solution for 30 min at 37°C followed by an amplification step of the hybridized labelled oligonucleotides for 100 min at 37°C with the polymerase solution. Slides were then covered with Duolink In Situ Mounting Medium with DAPI (Sigma-Aldrich by Merck) and coverslips. Nuclear foci were visualized using BZ-9000 microscope (Keyence, Cologne, Germany). Quantification was done with the BZ-II Analyzer software (Keyence).

In situ analysis of protein interactions at DNA replication forks

SIRF was conducted according to Petruk and colleagues (26,27) followed by PLA. First, cells were either grown in chamber slides or in case of suspension culture cells on plates. Then EdU (20 μM) was incorporated for 8 min followed by another incubation with thymidine (100 μM) for a chase period of up to 4 h. After pre-extraction (as described for PLA) and fixation with 2% methanol-free formaldehyde (Thermo Fisher Scientific, Waltham, MA, USA) permeabilization with 0.5% (v/v) Triton X-100 in PBS was followed by a click reaction (100 mM sodium-(L)-ascorbate, 2 mM $CuSO_4$ and 0.01 mM biotin azide in PBS). Afterwards the staining procedure was continued at the blocking step of the PLA. Primary antibodies were used as already described in the PLA paragraph in the Supplementary together with anti-biotin (mouse, B7653, Sigma-Aldrich by Merck, Darmstadt, Germany or rabbit, #5597, Cell Signaling, Danvers, MA, USA).

Statistics

Graphic presentation of data was carried out using GraphPad Prism 8 software. Data was shown as mean ± SEM or mean ± SD, as stated in the figure legends. For related values significances were calculated by Wilcoxon matched-pairs signed rank test (two-sided) whereas, for the other data Mann–Whitney *U* test (two-sided) was used, which was preceded by Kuskal–Wallis test when comparing groups with more than two samples.

RESULTS

The nascent DNA elongation rate is lower in SCs than in differentiated counterparts

Changes in the nascent DNA elongation rate affect genomic instability and cell death (28). However, its relevance for other biologically relevant outputs such as stemness has remained underexplored. Therefore, we examined nascent DNA replication rates in pairs of isogenic non-differentiated (nd) and differentiated (diff) samples. Human embryonic stem cells (hESCs) derived from the H9 cell line were differentiated into the neuronal lineage (ndiff) or spontaneously (sdiff), into the endoderm-like direction using pre-established procedures (29,30) (Figure 1A). The differentiation status of the cells was confirmed by assessing the levels of: (a) the pluripotency marker Nanog (12), (b) p53 (12) and (c) the neurogenesis marker paired box 6 (PAX6) (31) (Supplementary Figure S1A). Samples were subjected to DNA Fiber Spreading Assays (32) performed as reported by us before (25). Strikingly, DNA tracks in nd cells were shorter than in the two diff lineages (Figure 1B).

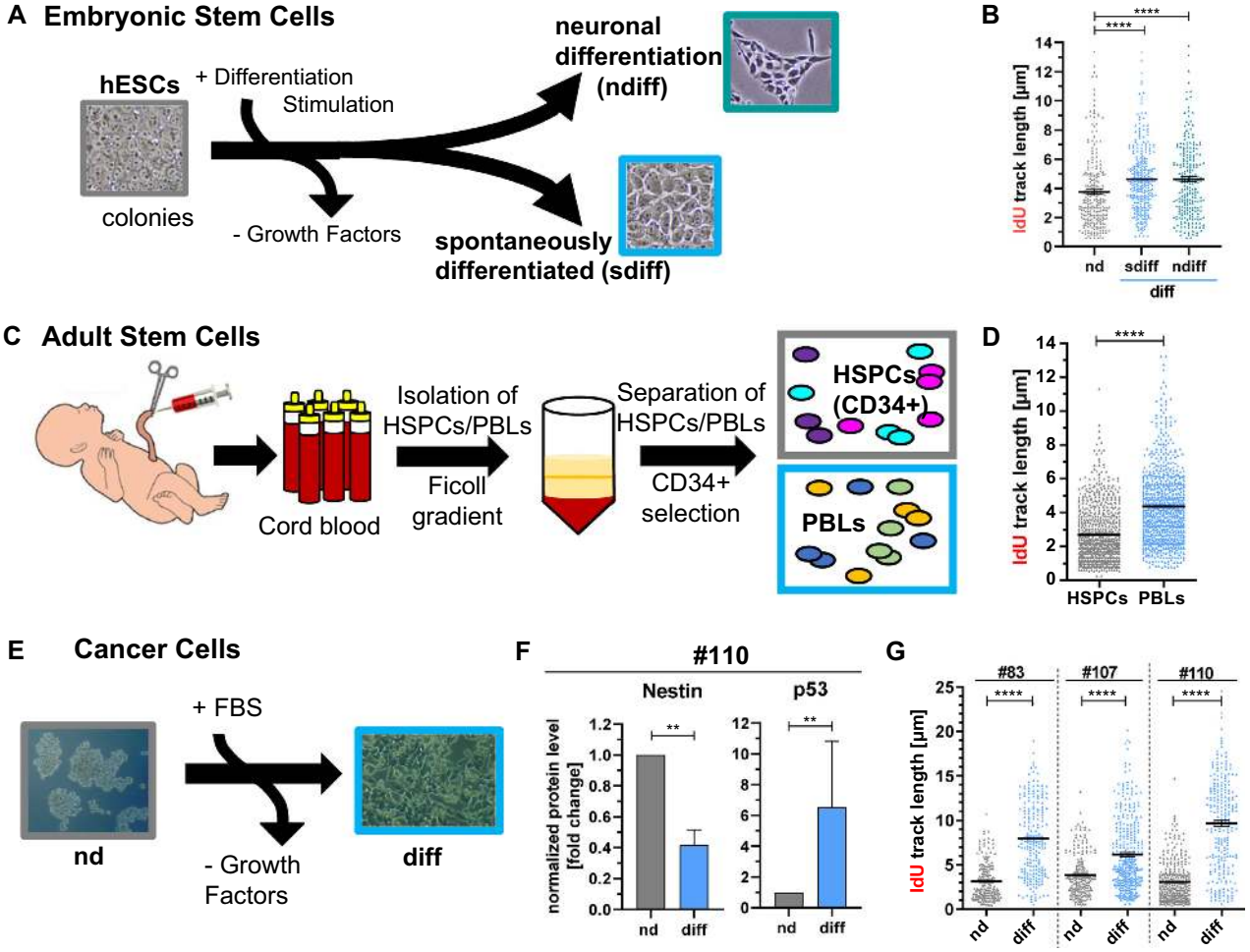

Figure 1. Nascent DNA elongation in SCs and their differentiated counterparts. Nascent DNA track lengths were measured after DNA Fiber Spreading Assays: sequential incorporation of CldU (20 min) and IdU (30 min) in B and G and of CldU (20min) and IdU (20 min) in D, results from two to three independent experiments. Only IdU track measurements from bi-colored fibers are depicted for clarity here but similar results were obtained when analyzing CldU tracks. In B, D, F, G: mean ± SEM. $^{**}P \leq 0.01$, $^{****}P \leq 0.0001$ (B, D, G: Mann–Whitney *U* test, two-sided F: Wilcoxon matched-pairs signed rank test, two-sided). (**A**) Schematic representation of differentiation of non-differentiated (nd) hESCs either spontaneously (sdiff) or into neuronal lineage (ndiff). (**B**) DNA Fiber Spreading Assay for nd hESCs, sdiff and ndiff cells (100–180 fibers/experiment). (**C**) Illustration of isolation of adult SCs (HSPCs) and differentiated cells (PBLs) from cord blood samples using a Ficoll gradient and HSPC enrichment by CD34 MicroBead Kit. (**D**) DNA Fiber Spreading Assay for HSPCs and PBLs from 1–5 donors/experiment (130–400 fibers/experiment). (**E**) Graphical presentation of differentiation of nd ovarian cancer cells to differentiated (diff) cells. (**F**) Western blot quantification of Nestin and p53 for ovarian cancer cell line #110. Individual band intensities were corrected by the corresponding ones for housekeeping genes (β-actin, GAPDH or PCNA) followed by normalization of protein levels to nd cells. Analysis was done for 9 (Nestin)–10 (p53) blots. (**G**) DNA Fiber Spreading Assay for three cell lines of ovarian cancer cells (#83, #107, #110) in the nd and diff status each (70–200 fibers/experiment).

Secondly, we compared cycling adult HSPCs and differentiated peripheral blood lymphocytes (PBLs) isolated from umbilical cord blood samples (Figure 1C). DNA tracks were on average shorter in HSPCs than in PBLs (Figure 1D). In agreement with its differentiation status, PBLs showed higher p53 levels than HSPCs (Supplementary Figure S1B). Thus, adult SCs also revealed a slower nascent DNA elongation rate than differentiated counterparts.

As a third line of evidence, a cancer SC model was explored. We used three cancer cell lines derived from ovarian tumors of three different patients (#83, #107, #110) enriched for tumor initiating cells (20). Such cell lines express wild-type p53 and grow as spheroids in their nd state exhibiting SC and EMT characteristics (20). The removal of growth factors and the addition of fetal bovine serum (FBS) causes the loss of SC and mesenchymal properties (20) (Figure 1E) as confirmed when monitoring relevant markers and p53 levels (Figure 1F, Supplementary Figure S1C–S1D). In all cases, DNA tracks were shorter in nd than in diff samples (Figure 1G, representative pictures for #110 in Supplementary Figure S1E). In conclusion, in embryonal, adult and cancer SC models, the differentiation status affects the rate of nascent DNA elongation.

Lower DNA elongation rates in SCs are accompanied by diminished replication stress

The shortening of replication tracks can be the consequence of increased origin firing. Common causes of increased origin firing are stalling and breakage of replication forks (33–

35). We therefore determined the frequency of active origins as done in the past (33,36) but found no significant difference between nd and diff cells (Supplementary Figure S1F). An additional source for track shortening is fork stalling, which can be indirectly revealed as fork asymmetry (28). As we did in the past (17), such a stalling parameter was determined by measuring the length of two IdU tracks emanating from the same origin (CldU track) (17). Interestingly, we found a significantly increased asymmetry in diff cells when compared to nd cells (Figure 2A), implying that the shorter tracks of nd cells are not the result of fork stalling and are more likely related to a slower replication rate.

In a next step, proliferation was examined, finding no major change (Supplementary Figure S1G). Given the better access to the samples, we focused for the further analysis of the mechanism on the cancer cell model. We then analyzed the cell cycle distribution by flow cytometry after propidium iodide staining and noticed a statistically significant increase of the percentage of G1 phase in nd cells when compared with diff cells (Supplementary Figure S1H). Moreover, we used a more sensitive method of sequential CldU/IdU incorporation to infer the time taken for the progression through S-phase (22), and observed a prolonged S-Phase in nd cells when compared to nd counterparts (Supplementary Figure S1I). These data suggested that nd cells enter and progress through S-phase more slowly than diff cells, which is in line with the observed slower replication speed in nd cells.

Knowing that replication-associated DNA damage load modulates DNA replication speed and vice versa (28,37), we monitored DDR markers such as γH2AX and 53BP1 foci accumulation (Figure 2B-C). Notably, unperturbed and mitomycin C (MMC)-treated diff cells displayed higher levels of γH2AX foci when compared to nd cells (Figure 2B, left panel). While the levels of 53BP1 foci were not equivalent to γH2AX foci (Figure 2B, central panel), colocalized γH2AX and 53BP1 foci (Figure 2B, right panel), indicating replication-associated DSBs (37), followed the γH2AX foci pattern. γH2AX foci were reported to label DNA lesions at sites of replication stress including but not limited to DSBs (38). 53BP1 was shown to play an important role in protecting reversed forks from uncontrolled restart and end resection (39,40). Therefore, the increase in γH2AX but not 53BP1 foci in diff cells may reflect replication stress associated with replication forks devoid of 53BP1 shielding and prone to ssDNA accumulation (41,42). Confirming that diff cells may be prone to ssDNA accumulation when compared to nd cells, immunoblot experiments revealed a sharp rise in the modified form of RPA in nd cells (phospho-RPA S33) that was hardly detected in nd cells (Figure 2D). Given that the Ataxia telangiectasia and Rad3 related serine/threonine kinase (ATR) phosphorylates histone H2AX at Ser139 and RPA32 at Ser33 in response to replication stress (43,44), we analyzed the activation of the upstream kinase by immunoblotting experiments. Phosphorylation of ATR at Ser428 (P-ATR) relative to total ATR rose in diff cells supporting the concept of enhanced replication stress in diff compared to nd cells (Figure 2E). These results suggested that, counterintuitively, the cells undergoing the highest replication stress (diff cells) are the ones synthesizing nascent DNA at a highest speed, perhaps as a consequence of a more efficient tolerance pathway choice.

p53 and POLι promote nascent DNA elongation in differentiated cells but slow down such a DNA synthesis in SC counterparts

The inverse correlation between replication stress markers and nascent DNA elongation rates in nd and diff cells suggests a different usage of DDT pathways. Hypothesizing that HSPCs use the p53- and POLι-dependent DDT pathway (17) we performed knockdown (kd) of p53 and POLι using previously validated si and shRNAs (17,42,45) (Figure 3, Supplementary Figure S2) and evaluated nascent DNA elongation. p53 and POLι kd caused track elongation in hESCs (Figure 3A), but shortening in both diff cell types (Figure 3A). p53 and POLι kd also affected the track lengths of the adult and cancer nd and diff cell models, with opposing effects depending on the differentiation status of the cells (Figure 3B–D). Underscoring the significance of the findings, such results were observed regardless of the use of siRNA or shRNA or the type of POLι shRNA and the degree of protein downregulation (Figure 3E, Supplementary Figure S2).

POLι acts in the same pathway as p53 and controls the activities of downstream partners in nascent DNA elongation of SCs and differentiated cells

While p53 in complex with POLι exerts a direct role in DDT affecting replication track lengths (17), p53 also interacts with other DNA repair/replication proteins and transcriptionally transactivates targets relevant for DDR (9,46). Hence, we examined the expression of such p53 targets and partners. The waterfall plot in Figure 4A summarizes densitometric quantifications of protein levels in diff relative to nd cancer cells (Western Blots: Figure 4B). p53 levels were the most different, followed by its target p21, POLι, the p53-inducible ribonucleotide-diphosphate reductase subunit M2 B (p53R2), polymerase eta (POLη) as well as HLTF, a component of the p53-dependent DDT pathway (17). The levels of DDT components PCNA and ZRANB3, the base excision repair (BER) enzymes apurinic/apyrimidinic endonuclease 1 (APE1) and DNA polymerase beta (POLβ), both p53 binding proteins as well as of another p53 target, the mouse double minute 2 homolog (MDM2) did not change when comparing nd and diff cells (Figure 3A). Of note, although both p53 and POLι are upregulated in diff cells, we did not find evidence of transcriptional regulation of POLι by p53 (Figure 4C).

Using previously validated shRNAs (17,47), we then tested the influence of individual kd of the above-mentioned proteins on the replication track length (Supplementary Figure S3A–H). The effects of protein kd could be separated in three groups: First, proteins which are not major players in track length elongation such as APE1 whose kd did not have an effect on DNA track lengths (black circles). Second, proteins affecting track length elongation in a similar fashion in nd and diff cells such as ZRANB3 and POLβ (black circles). Third, proteins, which regulate track length elongation with opposed effects in nd and diff cells.

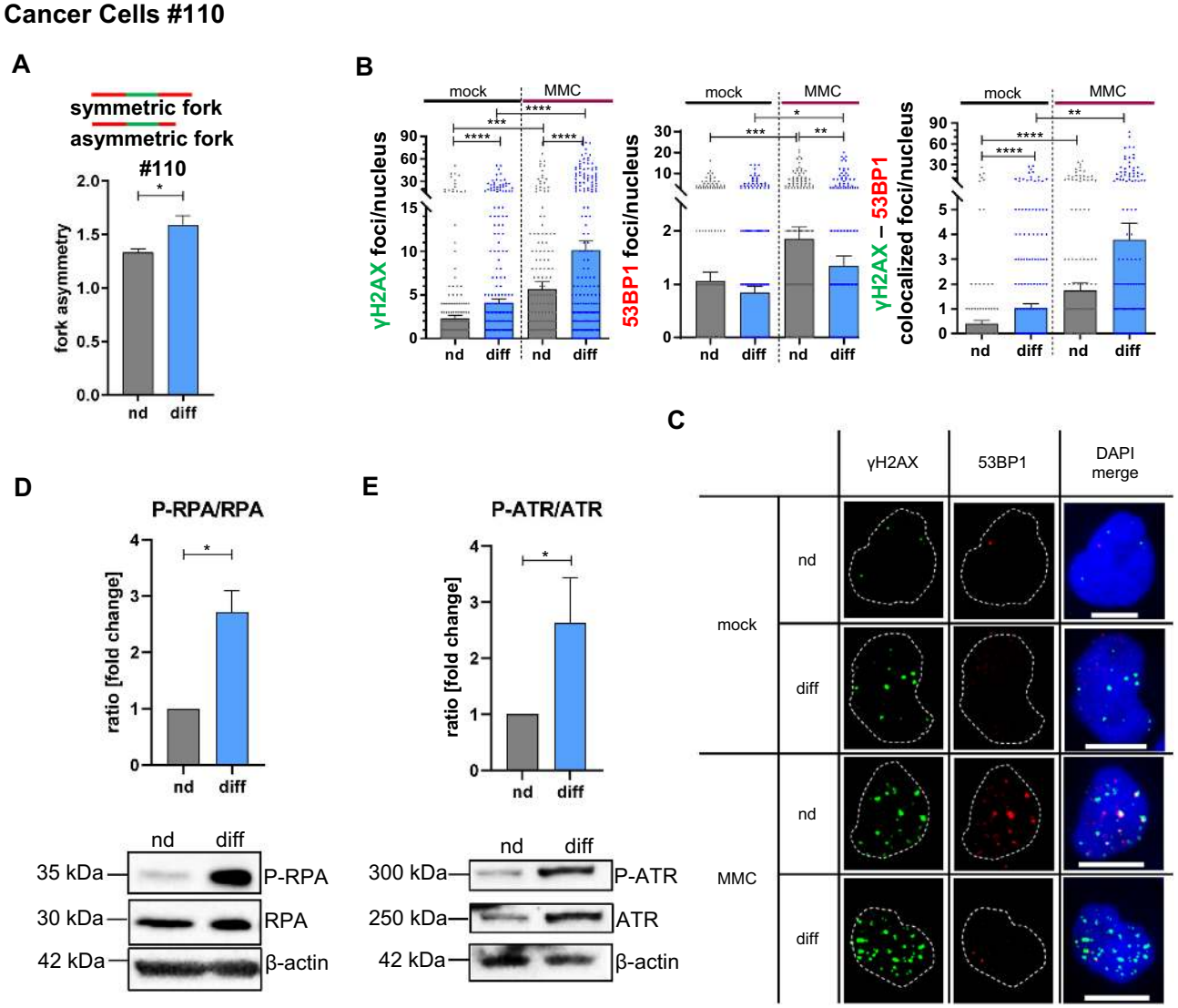

Figure 2. DNA damage in SCs and their differentiated counterparts. Various DNA damage markers were investigated in nd and diff ovarian cancer cells of line #110. Shown are mean ± SEM. $*P \leq 0.05$, $**P \leq 0.01$, $***P \leq 0.001$, $****P \leq 0.0001$ (A, B: Mann–Whitney *U* test, two-sided, D, E: Wilcoxon matched-pairs signed rank test, two-sided). (**A**) Fork asymmetry of cell line #110. Measured were IdU tracks emanating from the same origin (CldU track). Finally, the longer IdU track was divided by the shorter one. The ratio for nd and diff cells is displayed in the graph. (**B**) Foci analysis of γH2AX and 53BP1 as well as colocalized foci after solvent (mock) or mitomycin C (MMC) treatment. Cells were treated with solvent (H_2O) or 3 μM MMC for 45 min and then incubated for 3 h with medium until fixation. The graphs show the results from two independent experiments (120–200 cells/experiment). (**C**) Representative pictures of γH2AX, 53BP1 and colocalized foci after mock or MMC treatment. White scale bars: 10 μm. (**D**) and (**E**) show results of WB analysis and representative blots. *P–x* correspond to the phosphorylated forms of the indicated proteins. Individual band intensities were corrected to the corresponding ones for the housekeeping genes β-actin, ratios are formed of phosphorylated to basal proteins followed by normalization of protein levels to nd cells. RPA (D) corresponds to replication protein A and ATR (E) corresponds to Ataxia telangiectasia and Rad3 related serine/threonine kinase. Images are representative of 6 independent experiments.

Within the latter group, two sub-groups can be defined. The first sub-group includes p53, POLι, p21, p53R2 and MDM2 whose kd reduced replication track differences between nd and diff cells (green circles). The second sub-group covers POLη and HLTF whose kd further amplified the difference in DNA track lengths in the two cell types (magenta circles). Proteins in the third group could: (a) regulate the same DDT pathway in both cell types, but with diametrically opposed results in nd and diff cells or (b) contribute to different DDT pathways. These results also demonstrate that p53, its partners and targets differentially influence DNA elongation in nd and diff cells. They do so in a manner that does not, at least entirely, depend on the changes in protein expression levels of nd versus diff cells (compare with waterfall plot in Figure 4A).

To examine whether the effect of p53 is indirect and potentially dependent on TA of p21, we performed a double-kd of p53 and p21 (Figure 4D). The analysis of track lengths revealed an additive effect of p53 kd and p21 kd. While p53 kd or p21 kd alone resulted in a 1.2- to 1.4-fold increase in nd and a 20–30% decrease in diff cells (Figure 3C, Supplementary Figure S3A), the double-kd revealed a 1.7-fold

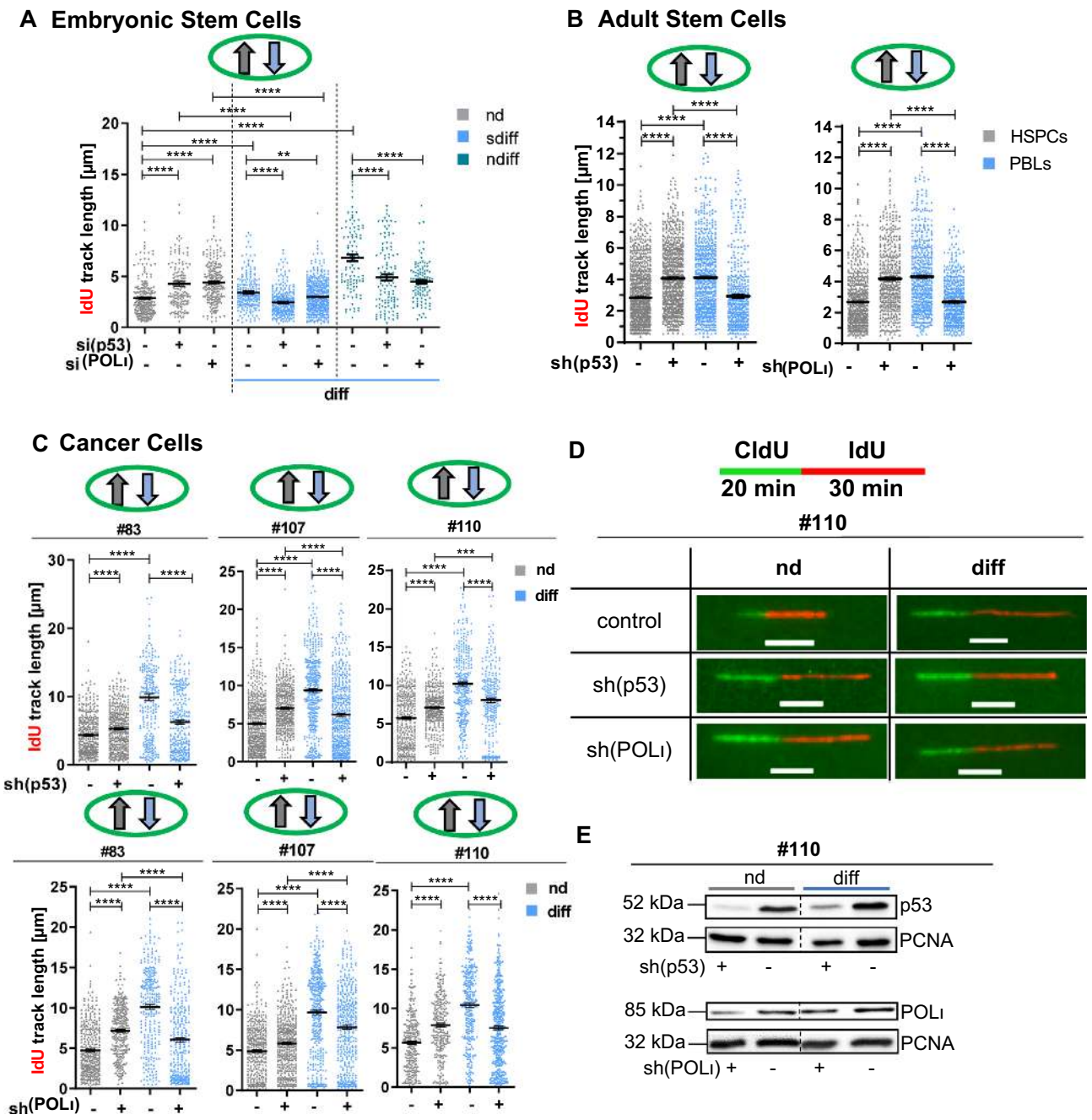

Figure 3. Impact of p53 and POLι expression on the average nascent DNA track length of SCs and differentiated cells. DNA Fiber Spreading Assays with sequential incorporation of CldU (20min) and IdU (30min) in A and C and of CldU (20min) and IdU (20min) in B after kd of p53 and POLι using gene specific shRNA (sh) or siRNA (si). As controls empty vectors without sh/with scrambled sh or non-silencing si were used. For clarity protein nomenclature was used for both genes and proteins throughout the manuscript. Experiments were conducted 24–48 h post-transfection. In (A–D): mean ± SEM. $^{**}P \leq 0.01$, $^{****}P \leq 0.0001$ (Mann–Whitney *U* test, two-sided). Arrows indicate the effect that a given kd causes on the average track length. Gray arrows: nd; blue: diff. Green circles encompass the following pattern caused by the kd: lengthening effect in nd, shortening effect in diff cells. (**A**) Results from hESCs (nd), differentiated into sdiff or ndiff after kd of p53 and POLι by si. Data shows IdU tracks from a representative experiment of two independent ones (100–380 fibers each). Statistics was calculated between single samples of the same lineage and between nd and diff lineages only. (**B**) DNA replication tracks in HSPCs and PBLs after kd of p53 and POLι by using sh. Results are the average of three independent experiments for 1–5 donors/experiment (120–530 fibers/experiment). (**C**) Replication phenotypes in ovarian cancer cell lines #83, #107 and #110 after kd of p53 and POLι using sh. Graphs depict results from two (#83, #110) or three (#107) independent experiments (#83: 110– 210, #107: 100–220, #110: 100–250 fibers/experiment). (**D**) Representative pictures of DNA fibers in ovarian cancer cell line #110. White scale bars: 5 µm. (**E**) Representative Western Blots after p53 and POLι kd, respectively, in cell line #110.

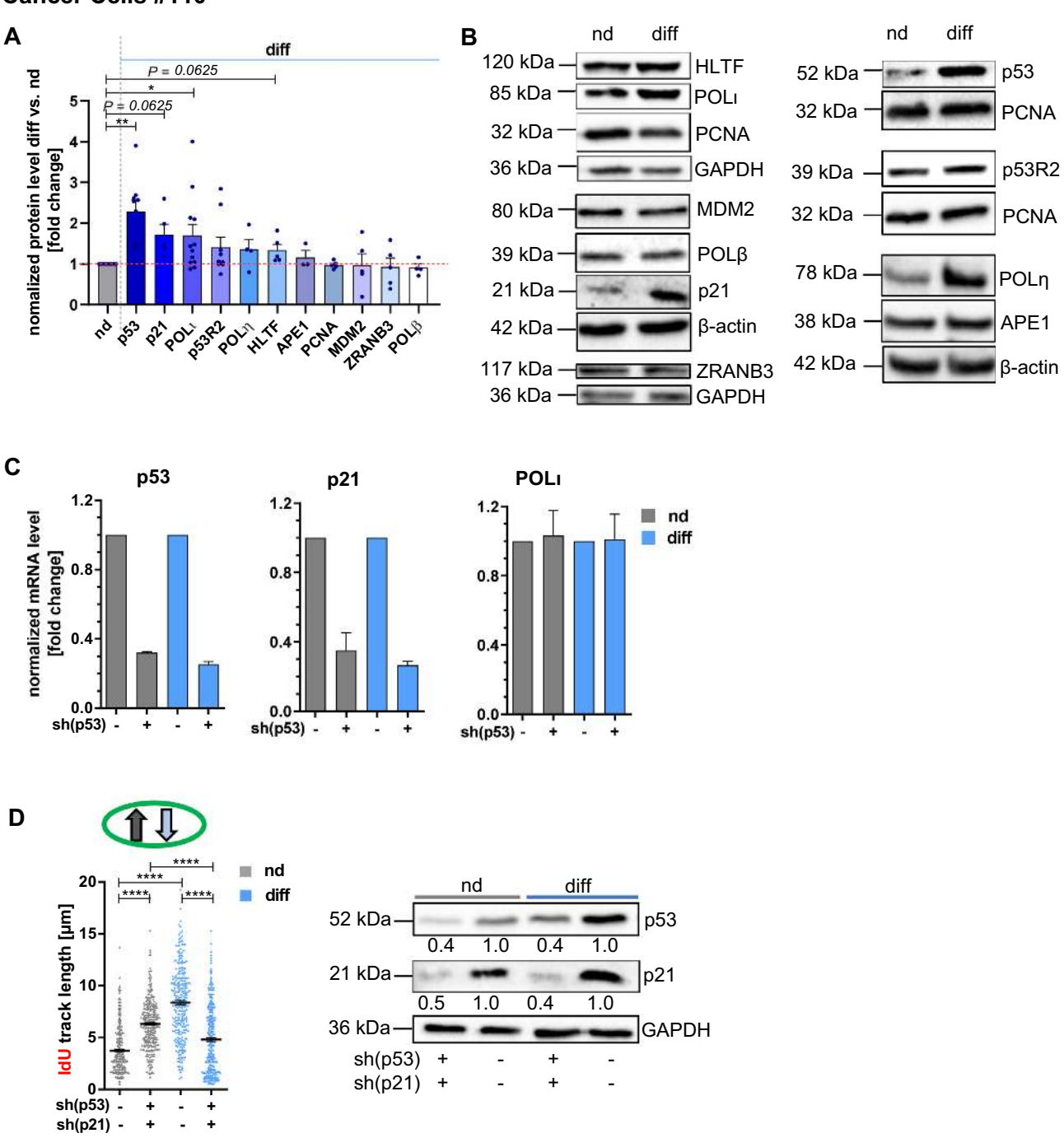

Figure 4. Effect of differentiation stage on protein expression and nascent DNA track length in ovarian cancer cells. For gene silencing vectors containing specific shRNAs (sh) or empty vectors without sh/with scrambled sh were transfected into cells. 24 h post-transfection experiments were conducted. In (A, D): mean ± SEM. $*P \leq 0.05$, $**P \leq 0.01$, $****P \leq 0.0001$ (A: Wilcoxon matched-pairs signed rank test, two-sided; D: Mann–Whitney *U* test, two-sided). In (C), mean ± SD. Arrows indicate the effect that a given kd causes on the average track length. Gray arrows: nd, blue: diff. Green circles encompass the following pattern caused by the kd: lengthening effect in nd and shortening effect in diff cells. (**A**). Western Blot analysis in nd and diff cells. Values were normalized to nd cells after individual corrections of band intensities with the ones from housekeeping genes (β-actin, GAPDH or PCNA) and then mean values sorted starting from the highest fold change (Waterfall plot). Quantification of 3 (APE1)–12 (POLι) blots. (**B**) Representative western Blots for (A). Black framed blots indicate origin from the same membrane and the same exposure. (**C**) Results of qRT-PCR from two independent experiments of #110 after p53 kd. For clarity the nomenclature for proteins was used throughout the manuscript. Investigated were mRNA levels of p53, p21 and POLι. Values were normalized to means of control samples for each cell line in each experiment. (**D**) Results of DNA Fiber Spreading Assays with sequential incorporation of CldU (20 min) and IdU (30 min) after double-kd of p53 and p21. Data shows IdU tracks from two independent experiments (130–180 fibers each).

track elongation in nd cells and in diff cells shortening by 40% (Figure 4D). Hence, both proteins exert at least partially independent functions during replication of both cell types.

Given that the replication phenotype observed in nd cells with DNA replication slow-down was reminiscent of the FR-DDT pathway triggered by the p53–POLι idling complex (17), we re-analyzed the fiber data obtained after kd of the key components of the pathway, i.e. POLι, p53 and ZRANB3 regarding fork asymmetries (Supplementary Figure S3I–K). Strikingly, kd of all three proteins raised asymmetries in nd cells to the elevated level observed in diff cells, while kd in diff cells did not further increase asymmetries. From this we conclude that POLι, p53 and ZRANB3 prevent fork stalling in nd cells by replication deceleration.

Next, we performed double-kd of POLι, p53, HLTF and ZRANB3 (Figure 5). Similar track length changes were observed after single and double-kd of POLι and p53 in both cell types suggesting that both proteins act in the same mechanisms (Figure 5A). Double-kd experiments targeting POLι together with HLTF (Figure 5B) or ZRANB3 (Figure 5C) caused track elongation in nd cells and shortening in diff cells in the range seen after single POLι kd (Figures 3C and 5A). These data indicated that POLι supports ZRANB3-dependent FR in nd cells, showing partial epistasis (compare results with Supplementary Figure S3H). In contrast in diff cells, where the effects of single POLι and ZRANB3 kd were opposite, the double-kd revealed the dominance of POLι, i.e. dependency of ZRANB3 function on POLι for track shortening. Dominance of POLι over the divergent, though moderate effects of HLTF (∼10%) (Supplementary Figure S3G), was revealed in both cell types (Figure 5B). These results substantiate epistatic relationships between POLι and p53 as well as between POLι and ZRANB3 in nd cells and unveiled that POLι is upstream of ZRANB3-mediated replication deceleration even in diff cells.

POLι selectively interacts with p53 and ZRANB3 in SCs

As POLι influenced the DDT pathway choices in nd and diff cells (Figure 2) and participates in p53-dependent (17), and independent DDT (48), we explored POLι protein complexes in nd and diff cells using *in situ* Proximity Ligation Assay (PLA). While POLι interacted with PCNA in both cell types (Figure 6A), it preferentially formed PLA foci with Ser15 phosphorylated p53 (P-p53), HLTF and ZRANB3 in nd cells (Figure 6B–D), whereas p21-POLι association was favored in diff cells (Figure 6E). The sketch in Figure 6F depicts the changes in the POLι complexes of nd vs. diff cells. Given that the homologous recombination factors BRCA2 and RAD51 have as well been implicated in fork protection (49) and fork reversal (50), respectively, we correspondingly investigated association of POLι with these proteins. While PLA foci indicated preferential association of POLι with RAD51 in nd cells (Supplementary Figure S4A), no differences were detected in PLA foci involving BRCA2 between the two cell types (Supplementary Figure S4B). These results supported the notion that nd but not diff cells efficiently engage the p53–POLι-mediated FR-DDT pathway.

Given the accepted role of POLι in translesion DNA synthesis (TLS) (51), a process triggered by PCNA mono-ubiquitination and aids track lengthening (52,53), it is possible that POLι supports TLS in diff cells. TLS is regulated by PCNA ubiquitination (53,54), and PCNA poly-ubiquitination, a post-translational modification that is particularly disfavored in diff compared with nd cells (Supplementary Figure S5A), inhibits TLS (55). Knockdown of p21, which colocalized with POLι in diff cells (Figure 6E) and was reported to modulate PCNA ubiquitination (56,57), selectively de-repressed poly-ubiquitination in diff cells (Supplementary Figure S5B), hence suggesting that POLι mediated TLS may be favored by the endogenous load of p21 in diff cells. Recruitment of TLS-POLι to DNA lesions can be detected by the formation of focal accumulations in the chromatin (61). Immunofluorescence microscopic analysis showed an increase of the average POLι foci numbers in diff compared with nd cells stemming from a rise of the percentage of cells with excess POLι foci (≥30 foci/cell) (Supplementary Figure S5C). Stress resistance is another hallmark of cells engaging TLS (59). Comparative assessment of cell viabilities revealed that POLι kd is significantly more detrimental to diff than to nd cells (Supplementary Figure S5D). These pieces of evidence support the likelihood that POLι promotes fast DNA synthesis by TLS in diff cells, where PCNA poly-ubiquitination is disfavored.

Chromatin immunoprecipitation after crosslinking (Co-IP) also revealed the p53–POLι and the PCNA-POLι interaction in nd cells (Figure 7A). The interaction of PCNA and POLι was not revealed in Co-IP experiments in diff cells, which may result from short residence times of TLS POLs at replication sites (60). Altogether, the IP data revealed the existence of different replication-relevant PCNA protein complexes in nd and diff cells, which most probably impact on the DDT pathway choice.

POLι and ZRANB3 are enriched at decelerated replication forks in SCs

To investigate if the protein complexes outlined in Figure 6 are associated with ongoing replication forks, we used *in situ* analysis of protein interactions at DNA replication forks (SIRF). This method combines EdU incorporation, click-it detection of nascent DNA and a PLA protocol, allowing detection of proteins enriched near/at ongoing replication forks (26,27). SIRF identifies these complexes at single-cell levels and can be advantageous when the amounts of cells are limited, as is the case when working with SCs at limited passage numbers. SIRF was performed with the POLι partners that revealed the most pronounced decline in diff versus nd cells in PLA assays, namely P-p53 and ZRANB3 (Figure 6B, D). First, levels of PCNA at the replication fork (EdU) and at post-replication sites (chase) were determined (Figure 7B). In line with the SIRF setting of Roy *et al.* (61) a selective localization of PCNA to active forks was observed. In nd cells, POLι was also found in the pulse fraction (Figure 7C), which was consistent with POLι-PCNA PLA data (Figure 6A), but was surprisingly maintained on DNA after the chase. Conversely, in diff cells POLι diminished in the chase fraction (Figure 7C). This result reveals a prolonged association of POLι with decelerated replication sites in nd

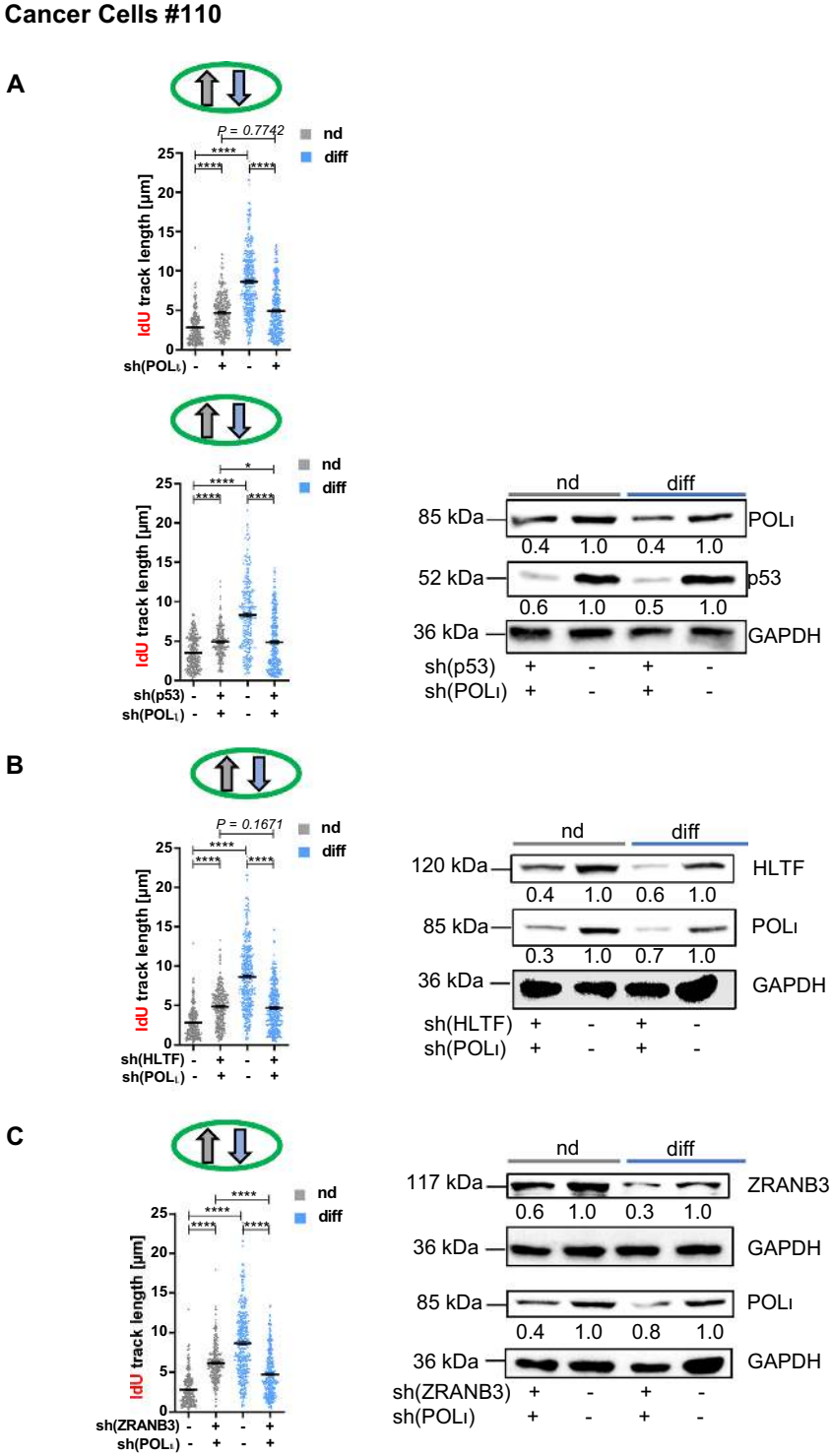

Figure 5. Effect of double-knockdown of POLι and candidate genes on nascent DNA track length in ovarian cancer cells. For gene silencing vectors containing specific shRNAs (sh) or scrambled control sh were transfected into cells. 24h post-transfection experiments were conducted. DNA Fiber Spreading Assays were performed by sequential incorporation of CldU (20min) and IdU (30min). In (A–C): mean ± SEM. *$P \leq 0.05$, ****$P \leq 0.0001$ (Mann–Whitney *U* test, two-sided). Arrows indicate the effect that a given kd causes on the average track length. Grey arrows: nd, blue: diff. Green circles encompass the following pattern caused by the kd: lengthening effect in nd and shortening effect in diff cells. (**A**) Results of DNA Fiber Spreading Assays after single kd of POLι and in parallel the double-kd of p53 and POLι and representative Western Blots. Data shows IdU tracks from two independent experiments (100–230 fibers each). (**B**) Results of DNA Fiber Spreading Assays after double-kd of HLTF and POLι and representative Western Blots. Data shows IdU tracks from two independent experiments (100–230 fibers each). (**C**) Results of DNA Fiber Spreading Assays after double-kd of ZRANB3 and POLι and representative Western Blots. Data shows IdU tracks from two independent experiments (100–230 fibers each). Please note, that kd experiments for POLι only and double-kd for POLι plus HLTF and POLι plus ZRANB3 as well as for the alternative POLι shRNA in Supplementary Figure S2D were performed simultaneously and therefore, correlated to the same control sample.

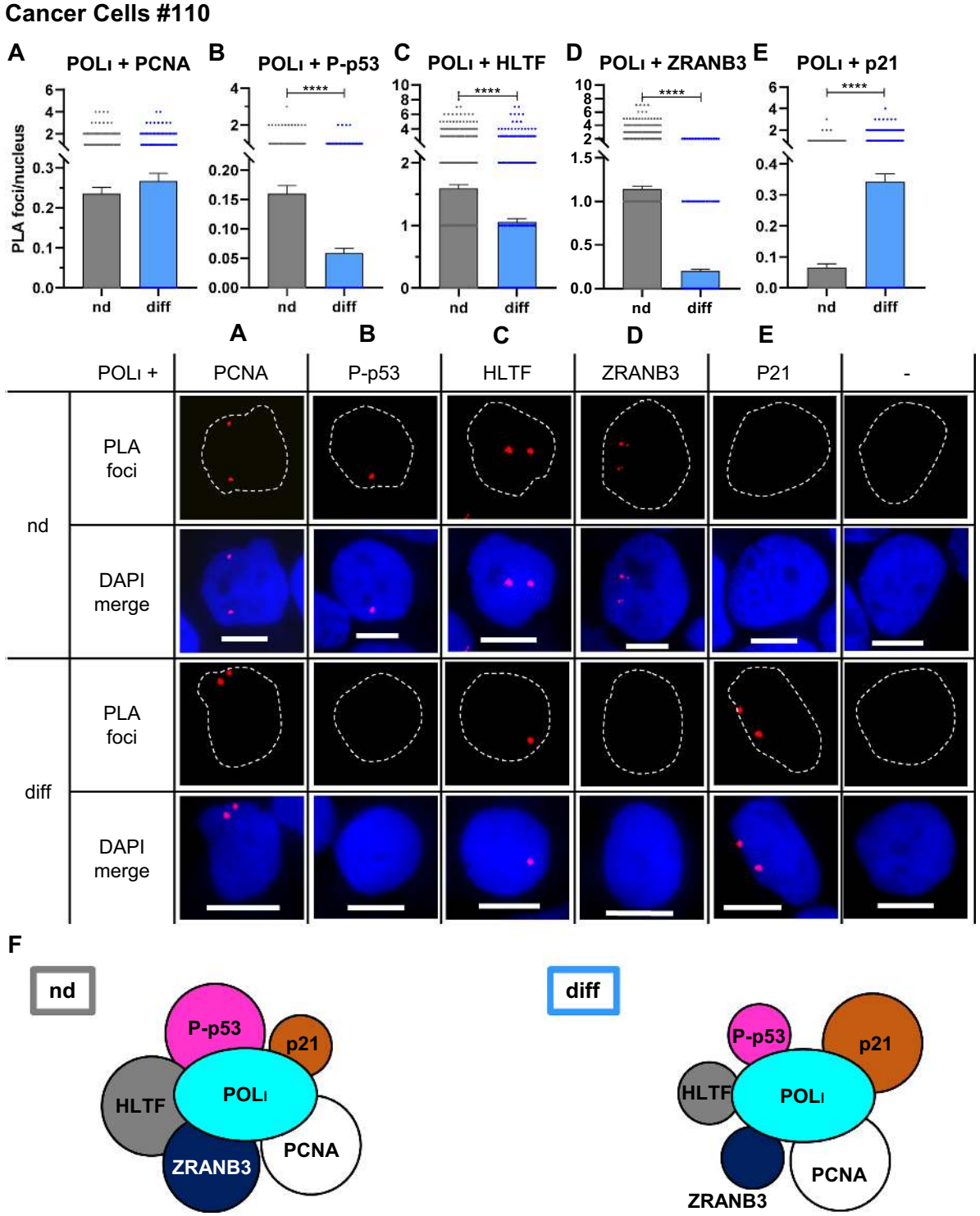

Figure 6. POLι association partners determined by proximity ligation assay in ovarian cancer cells. In (A), mean ± SEM. ****$P \leq 0.0001$ (Mann–Whitney U test, two-sided). White scale bars: 10 μm. PLA foci analysis of POLι and six other proteins within the nucleus of the cells. Shown are quantification and representative pictures for (**A**). POLι and PCNA (240–460 cells/experiment), (**B**) POLι and p53 phosphorylated at Ser15 (P-p53) (250–360 cells/experiment), (**C**) POLι and HLTF (210–350 cells/experiment), (**D**) POLι and ZRANB3 (120–420 cells/experiment), (**E**) POLι and p21 (230–310 cells/experiment). Last row of representative pictures corresponds to the negative control. (**F**) Schematic illustration of complex partners of POLι in nd (left panel) and diff (right panel) cells according to the quantitative results in (A–E), size of individual proteins correlates to their preference to interact with POLι in nd or diff cells; smaller size indicates relative decrease.

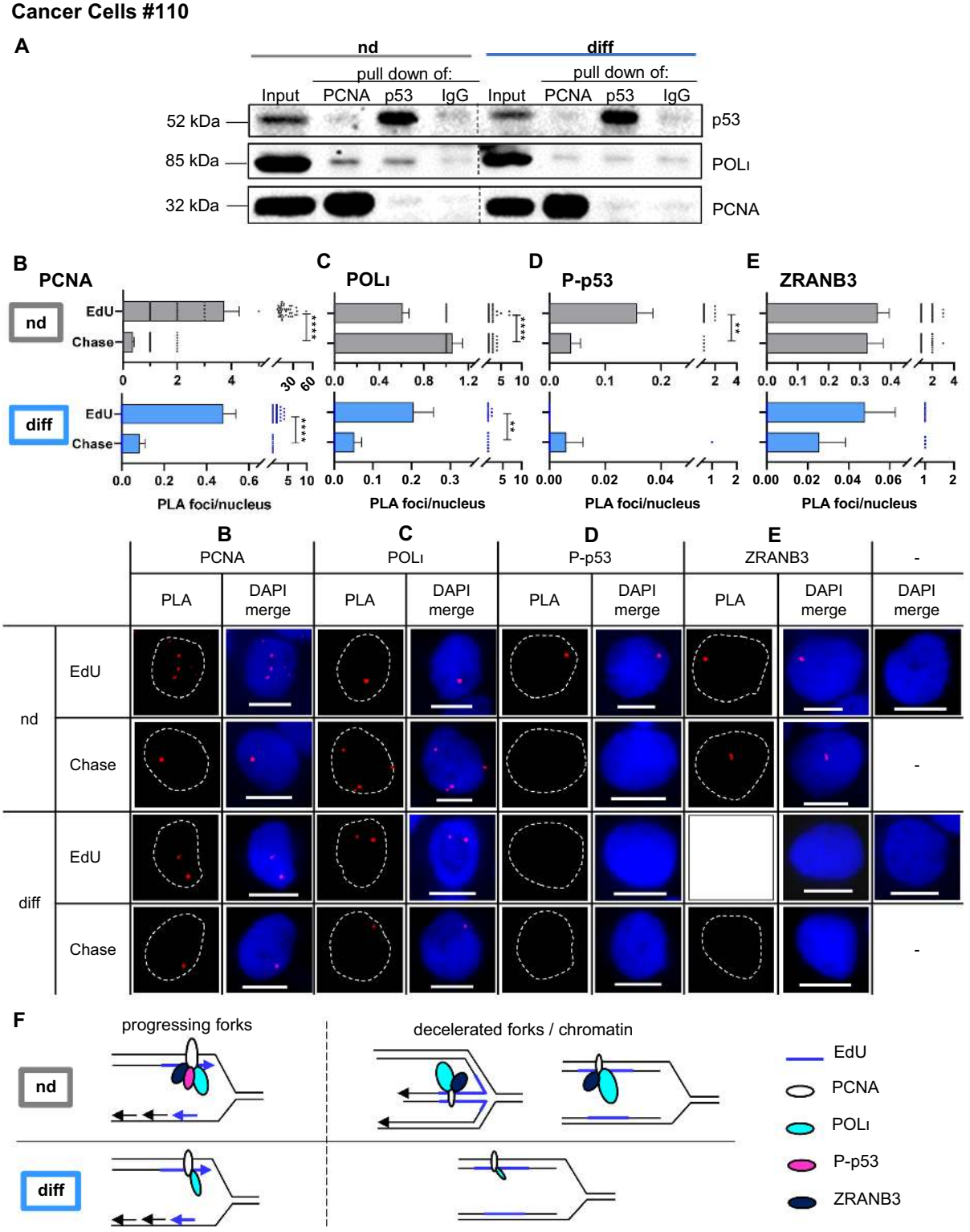

Figure 7. Protein complexes at progressing forks in nd and diff cells of ovarian cancer cells. In (B): mean±SEM. $^{**}P \leq 0.01$, $^{****}P \leq 0.0001$ (Mann–Whitney *U* test, two-sided). (**A**) Representative Co-IP. Black framed blots indicate origin from same membrane and same exposure. Stippled line implies cropping at this site. (B–E) Results of one out of two representative experiments of *in situ* analysis of protein complexes at DNA replication forks (SIRF). SIRF combines EdU incorporation (8 min) and the following chase (thymidine incorporation, ≤4 h) with a click reaction and a PLA, to detect proteins near/at ongoing replication forks. Grey columns (upper row): nd cells, blue columns (lower row): diff cells. Shown are also representative pictures (last column correlates to negative control). White scale bars: 10μm. Results for (**B**). PCNA (108–226 cells), for (**C**). POLι (88–316 cells), for (**D**). P-p53 (130–217 cells), for (**E**). ZRANB3 (148–291 cells). (**F**) Schematic illustration of protein complexes at nd and diff forks. Replisomes of nd cells are enriched in POLι, p53 and ZRANB3. During the chase, a fraction of the forks (PCNA positive) still binds POLι and ZRANB3, potentially revealing decelerating fork reversal events. Replisomes of diff cells are essentially devoid of p53 and ZRANB3. During the chase, PCNA and POLι are hardly detectable at forks.

cells, but a much more transient interaction in diff cells, which could reflect a more classical role in TLS. P-p53 was mainly present at the active fork in nd cells (Figure 7D) but its detection was very low in chased nd and in diff cells. The absence of P-p53 at progressing forks in diff cells implied that p53 does not directly participate in the DDT of these cells. ZRANB3 was detected at the active forks from nd cells and was equally prominent in the chase fraction (Figure 7E) supporting the POLι–ZRANB3 interaction revealed by the PLA (Figure 7D). The similarity in the POLι and ZRANB3 pattern suggests a common role in fork deceleration. In diff cells, almost no ZRANB3 foci were detected, implying that the participation of ZRANB3 in the DDT of these cells is more limited. Sketches in Figure 7F outline the interpretation of the results obtained in SIRF experiments. In nd cells, PCNA, POLι, P-p53 and ZRANB3 are located at active forks. After the chase, a POLι-ZRANB3 complex may be enriched at decelerated forks committed to FR. In diff cells, PCNA together with POLι were at active forks and to a much lesser extent in locations behind the forks implying that the differentiation status influences the choice between two different DDT pathways involving POLι.

DISCUSSION

While previous reports have acknowledged the role of DDT in the maintenance of the SC status, genome stability and cancer prevention (6) this report shows an association between the DDT pathway choice and the differentiation status. SCs select one particular DDT pathway to cope with endogenous replication stress while differentiated cells prioritize replication speed. Thus, SCs use a pathway depending on POLι, p53, PCNA, ZRANB3 and HLTF, which possibly leads to a DDT mediated by FR, whereas diff cells may rely predominantly on a more rapid DDT, possibly achieved by POLι-mediated TLS (Figure 8).

A physiological role of p53 in SCs that protects against DNA damage

In our work, human p53 levels were generally lower in SCs than in differentiated cells. In agreement, the TA activity of p53 was reported to be low in SCs (12,62,63) possibly avoiding counter-selecting mutations (63). Along with this observation, *TP53* was wild-type but TA targets such as p21 were low in the nd cell lines from ovarian cancer patients used in our study, which were enriched for tumor-initiating cells (20).

In addition, however, accumulating evidence indicates that despite being low, p53 is relevant for the physiology of SCs, in a manner that may or may not depend on its TA activity. First, ancestors of the p53 family protect the egg and sperm against DNA damage in invertebrates (63). Second, depending on the mouse strain, p53-deficiency correlates with developmental defects at birth (63). Third, in humans, p53 protects adult SCs (15). In particular, human HSCs need intact p53 to promote self-renewal (15). Loss of p53 was accompanied with increased spontaneous γH2AX foci, suggesting that the role of p53 in self-renewal was associated with DNA damage prevention (15). Reminiscent of this pattern, nd cells showed less DNA replication-associated damage than diff cells. Augmented replication speed could be at the source of the DNA damage of diff cells as recently suggested by Maya-Mendoza and colleagues (28). Therefore, it is conceivable that SCs enforce a mechanism to slow down at DNA replication barriers to reduce replication stress. In such a context, p53–POLι idling and ZRANB3-mediated FR (17) may represent an advantageous DDT choice in nd cells.

p53 and POLι directly control DNA damage tolerance to ensure slow fork progression in SCs

Herein we have presented evidence demonstrating that p53 and POLι negatively regulate the rate of nascent DNA synthesis in nd cells. The mechanism is reminiscent and builds upon our previous works (17,64), where we noticed that replication deceleration and homology-directed bypass of replication barriers are dependent on p53's exonuclease activity and p53–POLι complex formation. In analogy, we propose that such a pathway dominates the nascent DNA elongation program of nd cells, i.e. that POLι-polymerase and p53's exonuclease activities together mediate such a pathway choice by enabling idling events, which are iterative insertion and removal of nucleotides (18). By slowing fork progression, idling may generate a time-window that favors poly-ubiquitination of PCNA and thereafter recruitment of translocases. Our previous work has identified a crucial role of ZRANB3 among several tested translocases (SMARCAL1, BLM, WRN) in this newly discovered p53–POLι-mediated DDT pathway (17).

When assessing the contribution of different factors to the DNA replication speed control in nd and diff cells, we found that ZRANB3 decelerated DNA replication in both cell types, albeit with a smaller impact on diff cells. Given that ZRANB3 is a well-established translocase promoting transiently limited fork progression and dynamic FR (19,65,66), it is tempting to speculate that ZRANB3-dependent FR acts downstream of p53–POLι-mediated idling in nd cells, in particular (Figure 8). Double-kd experiments reinforce such a notion. In nd cells, POLι- and p53-mediated idling and ZRANB3-mediated fork slowing contribute to track length shortening. In diff cells, where the effects of single POLι and ZRANB3 kd were opposite, the double kd revealed dominance of POLι, i.e. ZRANB3-mediated DNA replication transactions being dependent on POLι also in these cells. From this we conclude that fork decelerating mechanisms are also active in diff cells and that POLι is upstream of those events as well. Unexpectedly, these data reveal that POLι is a master regulator of the differential DDT pathway choice (neutralizing the difference of track length between nd and diff cells and being essential for the activation of both lengthening and shortening tolerance pathway choices in both cell types).

The functional interaction of ZRANB3 and POLι in nd cells is also supported by PLA data. To a lesser extent this was also true for the E3 ligase HLTF and the recombinase RAD51, which are both also known to promote FR (50,59). Differently, BRCA2 showed the same association with POLι in both cell types, excluding a major role of homologous recombination or the fork protection function of BRCA2 acting on stalled rather than transiently reversed forks (49). Such observations suggest that while dynamic

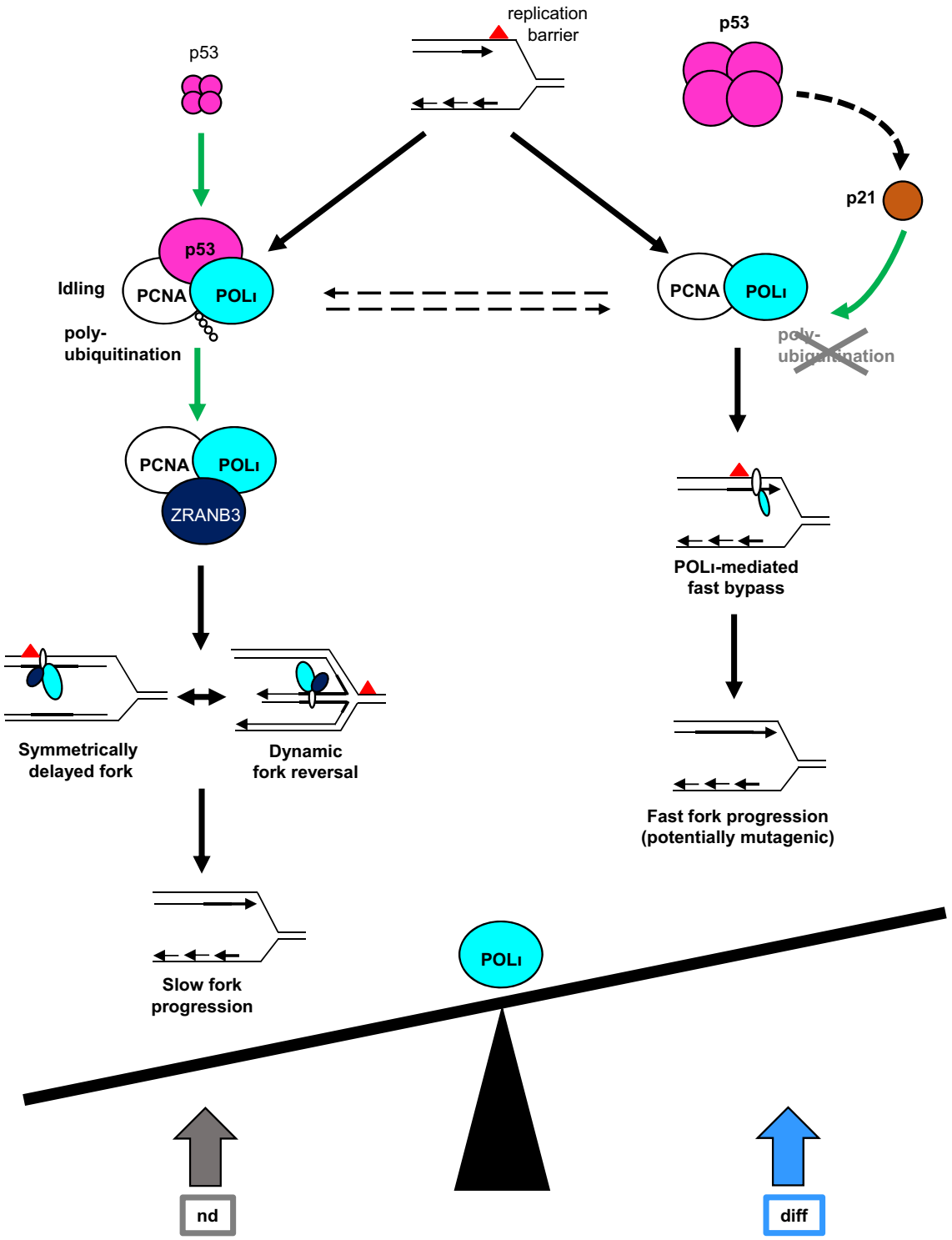

Figure 8. Model of replication bypass in nd and diff cells. In non-differentiated (nd) cells (left part of the model) a small amount of p53 is expressed (Figure 4A) supporting the p53–POLι idling-mediated DDT at DNA replication impediments (red triangle) (17). Once the p53–POLι complex associates with DNA (Figures 6A, B and 7C, D), idling events give extra time for PCNA poly-ubiquitination (Supplementary Figure S5A) promoting recruitment of downstream factors like ZRANB3 (Figures 6D and 7E) needed for symmetrically delaying forks and/or dynamic fork reversal altogether resulting in slow, but error-free fork progression (59,65). In diff cells, higher p53 levels induce higher levels of its transcriptional targets including p21 (Figure 4A). This change in protein expression supports a change in the pathway choice (right part of the model). In this cell type, p21 associates with PCNA (56,86) as well as POLι (Figure 6E) and antagonizes PCNA poly-ubiquitination (Supplementary Figure S5B), triggering another DDT choice, most likely TLS, which mediates rapid but potentially mutagenic bypass of the replication barrier (48). Though the TLS bypass is active also in nd cells and fork decelerating mechanisms also in diff cells (stippled thin arrows), POLι keeps the balance such that slow replication dominates in nd and fast replication in diff cells. Transcriptional transactivation by p53 is indicated by a stippled thick line. Green arrows in the model depict connections identified in this work, whereas black arrows indicate already published links.

FR can take place in both nd and diff cells, it would be favored by p53–POLι complexes in nd cells. Notably however, fork symmetry was high in nd cells in a manner depending on p53, POLι and ZRANB3, just like fork deceleration. This observation suggests that the decelerating mechanisms in nd cells act on both sides of the replication bubble with similar dynamics arguing against persisting FR at specific barriers. While previous work suggested that ZRANB3 decelerates DNA replication by dynamic, i.e. transient fork reversal (19), it is also conceivable that ZRANB3 as helicase or PCNA-stimulated endonuclease cooperates with the p53–POLι idling complex in nd cells (67). Future work will have to provide formal evidence for the impact of FR in p53-, POLι- and ZRANB3-dependent fork slowing in nd cells by quantitative electron microscopic imaging.

In differentiated cells POLι drives a diametrically opposed DNA damage tolerance pathway

In diff cells both p53 and POLι promoted high replication speed. This switch was accompanied with a major mechanistic change, as the interaction between both proteins was no longer required (as revealed in PLA and Co-IP experiments). The associations of ZRANB3, HLTF and RAD51 with POLι were also significantly reduced in diff cells, indicating that a different DDT pathway was favored.

POLι was reported to aid BER and key components of this pathway, POLβ and APE1, are interaction partners of p53 (68,69). APE1 kd did not reveal any influence on replication track lengths at all, POLβ silencing shortened DNA track lengths regardless of the differentiation status. Since APE1 is upstream of POLβ in the course of BER, the alterations in the DNA damage load after POLβ kd but not APE1 kd could influence the track lengths. Importantly, these data suggest that it is unlikely that POLι regulates DNA replication track lengths in nd and diff cells by BER functions.

So far, POLι has been underexplored in living cells, but biochemical data convincingly demonstrated that it can act as TLS polymerase (48). In general, if a specialized polymerase is depleted and the nascent DNA elongation resulting from the bypass of replication barriers is reduced, the involvement of the TLS polymerase in the successful bypass of the DNA lesion is inferred (52). Given that longer tracks in diff cells depended on POLι, we propose a role of POLι in TLS events in these cells. Additional support for this concept comes from our observations indicating that nuclear POLι foci were more readily formed and the pro-survival effects of POLι enhanced in diff cells. Altogether, these data support the concept of a shift towards enhanced TLS by POLι in diff cells.

The kd of POLη had the opposed effects on DNA tracks in nd and diff cells when compared to the kd of POLι. Though less pronounced, the effect of POLη kd was recapitulated by HLTF silencing. A likely explanation for the results after HLTF kd is that HLTF, as a ubiquitin E3 ligase and a translocase, supports several DDT pathways, including those involving SMARCAL1 instead of ZRANB3 (70). HLTF has also been described to stimulate both PCNA mono-ubiquitination and POLη-mediated TLS in a damage-specific manner (71). Hence, it is possible that the conditions for HLTF-mediated TLS by POLη are preferentially met in nd cells and for FR in diff cells. These alternative DDT pathways may compete with the p53–POLι-dependent one, resulting in net changes of replication tracks of only ∼10% after HLTF kd. Most importantly, DNA Fiber Spreading Assays after double-kd of POLι and HLTF revealed the same pattern and degree of replication track changes as in single POLι kd cells. These data show that POLι is required possibly upstream of the modest changes seen after single kd of HLTF, again underscoring the role of POLι as master regulator of the DDT choices in nd and diff cells.

The p53 target, p21, contributes to the choice of the DNA damage tolerance pathway

In the light of these diametrically opposed DNA replication phenotypes orchestrated by p53 in concert with POLι, it should be mentioned that both positive and negative roles of p53 on replication track elongation have been previously reported. As mentioned already, a role of p53 in track shortening was previously linked to the p53–POLι idling complex and not to TA (17,64). On the other hand, p53 was reported to lengthen replication tracks in a manner that was dependent on its TA activity (72,73). While the potential sources for such differences are many, it is tempting to highlight that the contrary observations recapitulate the opposed contribution of p53 to the DNA elongation rate of nd vs. diff cells.

p21, p53R2 and MDM2 have been ranked as the top transcriptional targets of p53 (74) and all three supported the POLι–dependent DDT pathway choices. MDM2 may contribute to the replication of nascent DNA in nd and diff cells via mechanisms such as interaction with DNA polymerases POLη (75) or POLε (76), chromatin remodelling (77,78) and R-loop suppression (79). p53R2 ensures the deoxynucleotide (dNTP) supply (80–82), which can explain track shortening in diff cells after p53R2 kd. The track lengthening effect after p53R2 kd in nd cells is more puzzling. It might be due to the imbalance of the ribonucleotide (rNTP)/dNTP ratio disfavoring POLι as compared with POLη (83,84), and compromising the exonuclease activity of p53 (85).

The p53 target p21 is well-known to play a multifaceted role in negatively and positively regulating DNA elongation and TLS, whereby its PCNA binding capacity is a prerequisite and its protein level of critical importance (28,36,56,58,86,87). Our single and double-kd experiments revealed that p21 exerts at least partially distinct functions from p53 in the DDT pathway choice. While in diff cells the formation of a POLι-p21 complex may facilitate the use of POLι for TLS, in nd cells p21 indirectly supports p53–POLι–mediated idling. Intriguingly, up- and down-modulation of p21 were reported to stimulate PCNA ubiquitination (56,57). Here, we observed that p21 counteracts poly-ubiquitination of PCNA in diff cells in particular, which is in line with reduced levels of poly-ubiquitinated PCNA in these cells. Given that PCNA is involved in TLS in its mono-ubiquitinated form and in FR-DDT in its poly-ubiquitinated form (53), these data strengthen the concept that POLι facilitates TLS in diff and FR-DDT in nd cells. Therefore, elevated levels of the p53 target gene product p21

in diff cells might play a decisive role in modulating the formation of POLι protein complexes. Altogether, we propose that ZRANB3 is recruited to PCNA at sites, where p53–POLι-mediated idling delays replication fork progression thereby promoting poly-ubiquitination (17), which is antagonized in diff cells because of a lack of p53–POLι-mediated idling and by an augmentation of p21 in diff cells (Figure 8).

CONCLUSIONS

Herein we report that the differentiation status leads to slow replication in SCs and fast replication in diff cells. Remarkably, p53 and POLι are key to both replication choices albeit because of different mechanisms. In SCs, p53 triggers an idling process in concert with POLι, giving the replication forks time to accumulate PCNA poly-ubiquitination and recruit factors such as ZRANB3 resulting in symmetrically delayed and/or dynamic FR-mediated slow-down of DNA replication, which is expected to be error-free (Figure 8, left part). In differentiated cells, p53 indirectly promotes p21-POLι association. PCNA-polyubiquitination is antagonized, most likely by p21, thereafter boosting DNA replication speed in a manner that depends on POLι, very likely by POLι-mediated TLS, which should be a mutagenic type of tolerance event (Figure 8, right part). Such a pathway choice may be relevant, as the choice of a safe bypass of replication barriers is particularly desirable for long-lived SCs with the potential of replenishing the pool of short-lived diff cells. This concept is in agreements with works by others revealing that fork remodeling prevents unrestrained replication driven by potentially mutagenic mechanisms like TLS (59,87). Our work highlights that the DNA replication program in SCs is not recapitulated in diff cells, thereby suggesting that selectively targeting the DDT pathway of SCs may be relevant for therapies targeting cancer cells bearing stem-cell-like features.

DATA AVAILABILITY

The datasets generated during and/or analyzed during the current study are available from the corresponding authors upon request.

SUPPLEMENTARY DATA

Supplementary Data are available at NAR Online.

ACKNOWLEDGEMENTS

We thank Helmut Pospiech for sharing his expertise regarding p53, Alexander Kleger for helpful discussions, Melanie Rall-Scharpf for help concerning HSPCs and PBLs and Sylvia Ritter for the opportunity to work in her lab as well as for advice.
Author contributions: M.I. designed and performed most experiments; experiments involving hESCs were jointly designed and performed by M.I. and I.S. M.I. analyzed data and wrote the manuscript. S.B. trained M.I., supported experimental design and data analysis. I.S., C.B. and G.D. contributed critical reagents and analyzed ESC and ovarian carcinoma data, respectively. M.D. and L.W. conceived the project. L.W. designed experiments, figure flow, analyzed and interpreted data and edited the manuscript. V.G. aided experimental design, data analysis and interpretation and edited the manuscript.

FUNDING

German Research Foundation (DFG) Grants Project B3 in Research Training Group GRK 2254 'Heterogeneity and evolution in solid tumors (HEIST)' (to L.W. and M.D.); German Cancer Aid, Priority Program 'Translational Oncology: DETECT CTC: Detection and characterization of circulating tumor cells and tumor markers in advanced breast cancer in the context of tumor heterogeneity within the DETECT study program' [70112504 to L.W.]; International Graduate School of Molecular Medicine, Ulm University (to M.I.); V.G. was supported by the Alexander von Humboldt Foundation during her extended stay in the Wiesmüller laboratory (Friedrich Wilhelm Bessel Award to V.G.); Italian Association for Cancer Research (AIRC) [IG ID19797 to D.G.]. Funding for open access charge: Deutsche Forschungsgemeinschaft, Project B3 in Research Training Group GRK 2254 "Heterogeneity and evolution in solid tumors (HEIST)".
Conflict of interest statement. None declared.

REFERENCES

1. Pieraccioli,M., Nicolai,S., Antonov,A., Somers,J., Malewicz,M., Melino,G. and Raschellà,G. (2016) ZNF281 contributes to the DNA damage response by controlling the expression of XRCC2 and XRCC4. *Oncogene*, **35**, 2592–2601.
2. Weyemi,U., Redon,C.E., Choudhuri,R., Aziz,T., Maeda,D., Boufraqech,M., Parekh,P.R., Sethi,T.K., Kasoji,M., Abrams,N. *et al.* (2016) The histone variant H2A.X is a regulator of the epithelial-mesenchymal transition. *Nat. Commun.*, **7**, 10711.
3. Mani,S.A., Guo,W., Liao,M.J., Eaton,E.N., Ayyanan,A., Zhou,A.Y., Brooks,M., Reinhard,F., Zhang,C.C., Shipitsin,M. *et al.* (2008) The epithelial-mesenchymal transition generates cells with properties of stem cells. *Cell*, **133**, 704–715
4. Rocha,C.R., Lerner,L.K., Okamoto,O.K., Marchetto,M.C. and Menck,C.F. (2013) The role of DNA repair in the pluripotency and differentiation of human stem cells. *Mutat. Res.*, **752**, 25–35.
5. Simonatto,M., Latella,L. and Puri,P.L. (2007) DNA damage and cellular differentiation: more questions than responses. *J. Cell Physiol.*, **213**, 642–648.
6. Pilzecker,B., Buoninfante,O.A. and Jacobs,H. (2019) DNA damage tolerance in stem cells, ageing, mutagenesis, disease and cancer therapy. *Nucleic Acids Res.*, **47**, 7163–7181.
7. Bañuelos,C.A., Banáth,J.P., MacPhail,S.H., Zhao,J., Eaves,C.A., O'Connor,M.D., Lansdorp,P.M. and Olive,P.L. (2008) Mouse but not human embryonic stem cells are deficient in rejoining of ionizing radiation-induced DNA double-strand breaks. *DNA Repair (Amst.)*, **7**, 1471–1483.
8. Lane,A.A. and Scadden,D.T. (2010) Stem cells and DNA damage: persist or perish? *Cell*, **142**: 360–362.
9. Gatz,S.A. and Wiesmuller,L. (2006) p53 in recombination and repair. *Cell Death Differ.*, **13**, 1003–1016.
10. Puisieux,A., Brabletz,T. and Caramel,J. (2014) Oncogenic roles of EMT-inducing transcription factors. *Nat. Cell Biol.*, **16**, 488–494.
11. Koifman,G., Aloni-Grinstein,R. and Rotter,V. (2019) p53 balances between tissue hierarchy and anarchy. *J. Mol. Cell Biol.*, **11**, 553–563.
12. Jain,A.K., Allton,K., Iacovino,M., Mahen,E., Milczarek,R.J., Zwaka,T.P., Kyba,M. and Barton,M.C. (2012) p53 regulates cell cycle and MicroRNAs to promote differentiation of human embryonic stem cells. *PLoS Biol.*, **10**, e1001268.

13. Eldridge,C.B., Allen,F.J., Crisp,A., Grandy,R.A., Vallier,L. and Sale,J.E. (2020) A p53-dependent checkpoint induced upon DNA damage alters cell fate during hiPSC differentiation. *Stem Cell Reports*, **15**, 827–835.
14. Hünten,S. and Hermeking,H. (2015) p53 directly activates cystatin D/CST5 to mediate mesenchymal-epithelial transition: a possible link to tumor suppression by vitamin D3. *Oncotarget*, **6**, 15842–15856.
15. Milyavsky,M., Gan,O.I., Trottier,M., Komosa,M., Tabach,O., Notta,F., Lechman,E., Hermans,K.G., Eppert,K., Konovalova,Z. *et al.* (2010) A distinctive DNA damage response in human hematopoietic stem cells reveals an apoptosis-independent role for p53 in self-renewal. *Cell Stem Cell*, **7**, 186–197
16. Gottifredi,V. and Wiesmüller,L. (2018) The tip of an iceberg: Replication-Associated functions of the tumor suppressor p53. *Cancers*, **10**, 250.
17. Hampp,S., Kiessling,T., Buechle,K., Mansilla,S.F., Thomale,J., Rall,M., Ahn,J., Pospiech,H., Gottifredi,V. and Wiesmüller,L. (2016) DNA damage tolerance pathway involving DNA polymerase ι and the tumor suppressor p53 regulates DNA replication fork progression. *Proc. Natl Acad. Sci. U.S.A.*, **113**, E4311–E4319.
18. Khare,V. and Eckert,K.A. (2002) The proofreading 3′→5′ exonuclease activity of DNA polymerases: a kinetic barrier to translesion DNA synthesis. *Mutat. Res.*, **510**, 45–54.
19. Vujanovic,M., Krietsch,J., Raso,M.C., Terraneo,N., Zellweger,R., Schmid,J.A., Taglialatela,A., Huang,J.W., Holland,C.L., Zwicky,K. *et al.* (2017) Replication fork slowing and reversal upon DNA damage require PCNA polyubiquitination and ZRANB3 DNA translocase activity. *Mol. Cell*, **67**, 882–890.
20. Ricci,F., Bernasconi,S., Perego,P., Ganzinelli,M., Russo,G., Bono,F., Mangioni,C., Fruscio,R., Signrelli,M., Broggini,M. and Damia,G. (2012) Ovarian carcinoma tumor-initiating cells have a mesenchymal phenotype. *Cell Cycle*, **11**, 1966–1976
21. Luft,S., Arrizabalaga,O., Kulish,I., Nasonova,E., Durante,M., Ritter,S. and Schroeder,I.S.(2017) Ionizing radiation alters human embryonic stem cell properties and differentiation capacity by diminishing the expression of activin receptors. *Stem Cells Dev.*, **26**, 341–352.
22. Charrasse,S., Gharbi-Ayachi,A., Burgess,A., Vera,J., Hached,K., Raynaud,P., Schwob,E., Lorca,T. and Castro,A. (2017) Ensa controls S-phase length by modulating Treslin levels. *Nat. Commun.*, **8**, 206.
23. Bi,X., Barkley,L.R., Slater,D.M., Tateishi,S., Yamaizumi,M., Ohmori,H. and Vaziri,C. (2006) Rad18 regulates DNA polymerase kappa and is required for recovery from S-phase checkpoint-mediated arrest. *Mol. Cell Biol.*, **26**, 3527–3540.
24. Ireno,I.C., Wiehe,R.S., Stahl,A.I., Hampp,S., Aydin,S., Troester,M.A., Selivanova,G. and Wiesmüller,L. (2014) Modulation of the poly (ADP-ribose) polymerase inhibitor response and DNA recombination in breast cancer cells by drugs affecting endogenous wild-type p53. *Carcinogenesis*, **35**, 2273–2282.
25. Speroni,J., Federico,M.B., Mansilla,S.F., Soria,G. and Gottifredi,V. (2012) Kinase-independent function of checkpoint kinase 1 (Chk1) in the replication of damaged DNA. *Proc. Natl Acad. Sci. U.S.A.*, **109**, 7344–7349.
26. Petruk,S., Sedkov,Y., Johnston,D.M., Hodgson,J.W., Black,K.L., Kovermann,S.K., Beck,S., Canaani,E., Brock,H.W. and Mazo,A. (2012) TrxG and PcG proteins but not methylated histones remain associated with DNA through replication. *Cell*, **150**, 922–933.
27. Petruk,S., Mariani,S.A., De Dominici,M., Porazzi,P., Minieri,V., Cai,J., Iacovitti,L., Flomenberg,N., Calabretta,B. and Mazo,A. (2017) Structure of nascent chromatin is essential for hematopoietic lineage specification. *Cell Rep.*, **19**, 295–306.
28. Maya-Mendoza,A., Moudry,P., Merchut-Maya,J.M., Lee,M., Strauss,R. and Bartek,J. (2018) High speed of fork progression induces DNA replication stress and genomic instability. *Nature*, **559**, 279–284.
29. Mayer,M., Arrizabalaga,O., Lieb,F., Ciba,M., Ritter,S. and Thielemann,C. (2018) Electrophysiological investigation of human embryonic stem cell derived neurospheres using a novel spike detection algorithm. *Biosens. Bioelectron.*, **100**, 462–468.
30. Murry,C.E. and Keller,G. (2008) Differentiation of embryonic stem cells to clinically relevant populations: lessons from embryonic development. *Cell*, **132**, 661–680.
31. Thakurela,S., Tiwari,N., Schick,S., Garding,A., Ivanek,R., Berninger,B. and Tiwari,V.K. (2016) Mapping gene regulatory circuitry of Pax6 during neurogenesis. *Cell Discov.*, **2**, 15045.
32. Jackson,D.A. and Pombo,A. (1998) Replicon clusters are stable units of chromosome structure: evidence that nuclear organization contributes to the efficient activation and propagation of S phase in human cells. *J. Cell Biol.*, **140**, 1285–1295.
33. González Besteiro,M.A., Calzetta,N.L., Loureiro,S.M., Habif,M., Bétous,R., Pillaire,M.J., Maffia,A., Sabbioneda,S., Hoffmann,J.S. and Gottifredi,V. (2019) Chk1 loss creates replication barriers that compromise cell survival independently of excess origin firing. *EMBO J.*, **38**, e101284.
34. Petermann,E., Woodcock,M. and Helleday,T. (2010) Chk1 promotes replication fork progression by controlling replication initiation. *Proc. Natl Acad. Sci. U.S.A.*, **107**, 16090–16095.
35. Técher,H., Koundrioukoff,S., Carignon,S., Wilhelm,T., Millot,G.A., Lopez,B.S., Brison,O. and Debatisse,M. (2016) Signaling from Mus81-Eme2-Dependent DNA damage elicited by Chk1 deficiency modulates replication fork speed and origin usage. *Cell Rep.*, **14**, 1114–1127.
36. Mansilla,S.F., Bertolin,A.P., Bergoglio,V., Pillaire,M.J., González Besteiro,M.A., Luzzani,C., Miriuka,S.G., Cazaux,C., Hoffmann,J.S. and Gottifredi,V. (2016) Cyclin Kinase-independent role of p21CDKN1A in the promotion of nascent DNA elongation in unstressed cells. *Elife*, **5**, e18020.
37 Neelsen,K.J., Zanini,I.M.Y., Mijic,S., Herrador,Q., Zellweger,R., Chaudhuri,A.R., Creavin,K.D., Blow,J.J. and Lopes,M. (2013) Deregulated origin licensing leads to chromosomal breaks by rereplication of a gapped DNA template. *Genes Dev.*, **27**, 2537–2542.
38. Gagou,M.E., Zuazua-Villar,P. and Meuth,M. (2010) Enhanced H2AX phosphorylation, DNA replication fork arrest, and cell death in the absence of Chk1. *Mol. Biol. Cell*, **21**, 739–752.
39. Her,J., Ray,C., Altshuler,J., Zheng,H. and Bunting,S.F. (2018) 53BP1 mediates ATR-Chk1 signaling and protects replication forks under conditions of replication stress. *Mol. Cell Biol.*, **38**, e00472-17.
40. Mirza-Aghazadeh-Attari,M., Mohammadzadeh,A., Yousefi,B., Mihanfar,A., Karimian,A. and Majidinia,M. (2019) 53BP1: A key player of DNA damage response with critical functions in cancer. *DNA Repair (Amst.)*, **73**, 110–119.
41. Ahuja,A.K., Jodkowska,K., Teloni,F., Bizard,A.H., Zellweger,R., Herrador,R., Ortega,S., Hickson,I.D., Altmeyer,M., Mendez,J. and Lopes,M. (2016) A short G1 phase imposes constitutive replication stress and fork remodelling in mouse embryonic stem cells. *Nat. Commun.*, **7**, 10660.
42. Liu,W., Krishnamoorthy,A., Zhao,R. and Cortez,D. (2020) Two replication fork remodeling pathways generate nuclease substrates for distinct fork protection factors. *Sci. Adv.*, **6**, eabc3598.
43. Ward,I.M. and Chen,J. (2001) Histone H2AX is phosphorylated in an ATR-dependent manner in response to replicational stress. *J. Biol. Chem.*, **276**, 47759–47762.
44. Shiotani,B., Nguyen,H.D., Håkansson,P., Maréchal,A., Tse,A., Tahara,H. and Zou,L. (2013) Two distinct modes of ATR activation orchestrated by Rad17 and Nbs1. *Cell Rep.*, **3**, 1651–1662.
45. Gole,B., Mian,E., Rall,M. and Wiesmüller,L. (2018) Base excision repair proteins couple activation-induced cytidine deaminase and endonuclease G during replication stress-induced MLL destabilization. *Leukemia*, **32**, 159–167.
46. Sengupta,S. and Harris,C.C. (2005) p53: traffic cop at the crossroads of DNA repair and recombination. *Nat. Rev. Mol. Cell Biol.*, **6**, 44–55.
47. Brummelkamp,T.R., Bernards,R. and Agami,R. (2002) A system for stable expression of short interfering RNAs in mammalian cells. *Science*, **296**, 550–553.
48. McIntyre,J. (2020) Polymerase iota - an odd sibling among Y family polymerases. *DNA Repair (Amst.)*, **86**, 102753.
49. Schlacher,K., Christ,N., Siaud,N., Egashira,A., Wu,H. and Jasin,M. (2011) Double-strand break repair-independent role for BRCA2 in blocking stalled replication fork degradation by MRE11. *Cell*, **145**, 529–542.
50. Zellweger,R., Dalcher,D., Mutreja,K., Berti,M., Schmid,J.A., Herrador,R., Vindigni,A. and Lopes,M. (2015) Rad51-mediated replication fork reversal is a global response to genotoxic treatments in human cells. *J. Cell Biol.*, **208**, 563–579.

51. Sale,J.E. (2013) Translesion DNA synthesis and mutagenesis in eukaryotes. *Cold Spring Harb. Perspect. Biol.*, **5**, a012708.
52. Bertolin,A.P., Mansilla,S.F. and Gottifredi,V. (2015) The identification of translesion DNA synthesis regulators: Inhibitors in the spotlight. *DNA Repair (Amst.)*, **32**, 158–164.
53. Tonzi,P. and Huang,T.T. (2019) Role of Y-family translesion DNA polymerases in replication stress: Implications for new cancer therapeutic targets. *DNA Repair (Amst.)*, **78**, 20–26.
54. Moldovan,G.L., Pfander,B. and Jentsch,S. (2007) PCNA, the maestro of the replication fork. *Cell*, **129**, 665–679.
55. Chiu,R.K., Brun,J., Ramaekers,C., Theys,J., Weng,L., Lambin,P., Gray,D.A. and Wouters,B.G. (2006) Lysine 63-polyubiquitination guards against translesion synthesis-induced mutations. *PLos Genet.*, **2**, e116.
56. Avkin,S., Sevilya,Z., Toube,L., Geacintov,N., Chaney,S.G., Oren,M. and Livneh,Z. (2006) p53 and p21 regulate error-prone DNA repair to yield a lower mutation load. *Mol. Cell*, **22**, 407–413.
57. Soria,G., Podhajcer,O., Prives,C. and Gottifredi,V. (2006) P21Cip1/WAF1 downregulation is required for efficient PCNA ubiquitination after UV irradiation. *Oncogene*, **25**, 2829–2838.
58. Mansilla,S.F., Soria,G., Vallerga,M.B., Habif,M., Martínez-López,W., Prives,C. and Gottifredi,V. (2013) UV-triggered p21 degradation facilitates damaged-DNA replication and preserves genomic stability. *Nucleic Acids Res.*, **41**, 6942–6951.
59. Bai,G., Kermi,C., Stoy,H., Schiltz,C.J., Bacal,J., Zaino,A.M., Hadden,M.K., Eichman,B.F., Lopes,M. and Cimprich,K.A. (2020) HLTF promotes fork reversal, limiting replication stress resistance and preventing multiple mechanisms of unrestrained DNA synthesis. *Mol. Cell*, **78**, 1237–1251.
60. Solovjeva,L., Svetlova,M., Sasina,L., Tanaka,K., Saijo,M., Nazarov,I., Bradbury,M. and Tomilin,N. (2005) High mobility of flap endonuclease 1 and DNA polymerase eta associated with replication foci in mammalian S-phase nucleus. *Mol. Biol. Cell*, **16**, 2518–2528.
61. Roy,S., Tomaszowski,K.H., Luzwick,J.W., Park,S., Li,J., Murphy,M. and Schlacher,K. (2018) p53 orchestrates DNA replication restart homeostasis by suppressing mutagenic RAD52 and POLθ pathways. *Elife*, **7**, e31723.
62. Lee,D.F., Su,J., Ang,Y.S., Carvajal-Vergara,X., Mulero-Navarro,S., Pereira,C.F., Gingold,J., Wang,H.L., Zhao,R., Sevilla,A. *et al.* (2012) Regulation of embryonic and induced pluripotency by aurora kinase-p53 signaling. *Cell Stem. Cell*, **11**, 179–194.
63. Levine,A.J., Puzio-Kuter,A.M., Chan,C.S. and Hainaut,P. (2016) The role of the p53 protein in stem-cell biology and epigenetic regulation. *Cold Spring Harb. Perspect. Med.*, **6**, a026153.
64. Biber,S., Pospiech,H., Gottifredi,V. and Wiesmüller,L. (2020) Multiple biochemical properties of the p53 molecule contribute to activation of polymerase iota-dependent DNA damage tolerance. *Nucleic Acids Res.*, **48**, 12188–12203.
65. Ciccia,A., Nimonkar,A.V., Hu,Y., Hajdu,I., Achar,Y.J., Izhar,L., Petit,S.A., Adamson,B., Yoon,J.C., Kowalczykowski,S.C., Livingston,D.M., Haracska,L. and Elledge,S.J. (2012) Polyubiquitinated PCNA recruits the ZRANB3 translocase to maintain genomic integrity after replication stress. *Mol. Cell*, **47**, 396–409.
66. Bétous,R., Couch,F.B., Mason,A.C., Eichman,B.F., Manosas,M. and Cortez,D. (2013) Substrate-selective repair and restart of replication forks by DNA translocases. *Cell Rep.*, **3**, 1958–1969.
67. Sebesta,M., Cooper,C.D.O., Ariza,A., Carnie,C.J. and Ahel,D. (2017) Structural insights into the function of ZRANB3 in replication stress response. *Nat. Commun.*, **8**, 15847.
68. Gaiddon,C., Moorthy,N.C. and Prives,C. (1999) Ref-1 regulates the transactivation and pro-apoptotic functions of p53 in vivo. *EMBO J.*, **18**, 5609–5621.
69. Zhou,J., Ahn,J., Wilson,S.H. and Prives,C. (2001) A role for p53 in base excision repair. *EMBO J.*, **20**, 914–923.
70. Poole,L.A. and Cortez,D. (2017) Functions of SMARCAL1, ZRANB3, and HLTF in maintaining genome stability. *Crit. Rev. Biochem. Mol. Biol.*, **52**, 696–714.
71. Lin,J.R., Zeman,M.K., Chen,J.Y., Yee,M.C. and Cimprich,K.A. (2011) SHPRH and HLTF act in a damage-specific manner to coordinate different forms of postreplication repair and prevent mutagenesis. *Mol. Cell*, **42**, 237–249.
72. Klusmann,I., Rodewald,S., Müller,L., Friedrich,M., Wienken,M., Li,Y., Schulz-Heddergott,R. and Dobbelstein,M. (2016) p53 activity results in DNA replication fork processivity. *Cell Rep.*, **17**, 1845–1857.
73. Yeo,C.Q.X., Alexander,I., Lin,Z., Lim,S., Aning,O.A., Kumar,R., Sangthongpitag,K., Pendharkar,V., Ho,V.H.B. and Cheok,C.F. (2016) p53 maintains genomic stability by preventing interference between transcription and replication. *Cell Rep.*, **15**, 132–146.
74. Fischer,M. (2017) Census and evaluation of p53 target genes. *Oncogene*, **36**, 3943–3956.
75. Jung,Y.S., Qian,Y. and Chen,X. (2012) DNA polymerase eta is targeted by Mdm2 for polyubiquitination and proteasomal degradation in response to ultraviolet irradiation. *DNA Repair (Amst.)*, **11**, 177–184.
76. Vlatkovic,N., Guerrera,S., Li,Y., Linn,S., Haines,D.S. and Boyd,M.T. (2000) MDM2 interacts with the C-terminus of the catalytic subunit of DNA polymerase epsilon. *Nucleic Acids Res.*, **28**, 3581–3586.
77. Wienken,M., Dickmanns,A., Nemajerova,A., Kramer,D., Najafova,Z., Weiss,M., Karpiuk,O., Kassem,M., Zhang,Y., Lozano,G. *et al.* (2016) MDM2 associates with polycomb repressor complex 2 and enhances stemness-promoting chromatin modifications independent of p53. *Mol. Cell*, **61**, 68–83.
78. Alabert,C. and Groth,A. (2012) Chromatin replication and epigenome maintenance. *Nat. Rev. Mol. Cell Biol.*, **13**, 153–167.
79. Klusmann,I., Wohlberedt,K., Magerhans,A., Teloni,F., Korbel,J.O., Altmeyer,M. and Dobbelstein,M. (2018) Chromatin modifiers Mdm2 and RNF2 prevent RNA:DNA hybrids that impair DNA replication. *Proc. Natl Acad. Sci. USA*, **115**, E11311–E11320.
80. Guittet,O., Håkansson,P., Voevodskaya,N., Fridd,S., Gräslund,A., Arakawa,H., Nakamura,Y. and Thelander,L. (2001) Mammalian p53R2 protein forms an active ribonucleotide reductase in vitro with the R1 protein, which is expressed both in resting cells in response to DNA damage and in proliferating cells. *J. Biol. Chem.*, **276**, 40647–40651.
81. Niida,H., Shimada,M., Murakami,H. and Nakanishi,M. (2010) Mechanisms of dNTP supply that play an essential role in maintaining genome integrity in eukaryotic cells. *Cancer Sci.*, **101**: 2505–2509.
82. Wright,J.A., Chan,A.K., Choy,B.K., Hurta,R.A., McClarty,G.A. and Tagger,A.Y. (1990) Regulation and drug resistance mechanisms of mammalian ribonucleotide reductase, and the significance to DNA synthesis. *Biochem. Cell Biol.*, **68**, 1364–1371.
83. Vaisman,A. and Woodgate,R. (2018) Ribonucleotide discrimination by translesion synthesis DNA polymerases. *Crit. Rev. Biochem. Mol. Biol.*, **53**, 382–402.
84. Meroni,A., Nava,G.M., Bianco,E., Grasso,L., Galati,E., Bosio,M.C., Delmastro,D., Flaconi,M.M. and Lazzaro,F. (2019) RNase H activities counteract a toxic effect of Polymerase η in cells replicating with depleted dNTP pools. *Nucleic Acids Res.*, **47**, 4612–4623
85. Lilling,G., Elena,N., Sidi,Y. and Bakhanashvili,M. (2003) p53-associated 3′→5′ exonuclease activity in nuclear and cytoplasmic compartments of cells. *Oncogene*, **22**, 233–245.
86. Mansilla,S.F., de la Vega,M.B., Calzetta,N.L., Siri,S.O. and Gottifredi,V. (2020) CDK-Independent and PCNA-Dependent functions of p21 in DNA replication. *Genes (Basel)*, **11**, E596.
87. Nayak,S., Calvo,J.A., Cong,K., Peng,M., Berthiaume,E., Jackson,J., Zaino,A.M., Vindigni,A., Hadden,M.K. and Cantor,S.B. (2020) Inhibition of the translesion synthesis polymerase REV1 exploits replication gaps as a cancer vulnerability. *Sci. Adv.*, **6**, eaaz7808.